Dear reviewer,

Thank you very much for your valuable remarks, comments and suggestions. We find that by answering your questions and comments, and by following your suggestions, we have improved the readability of our work.

We start by answering the points raised in your general comment and then proceed with the section-specific suggestions/corrections.

In this document, your original comments are framed by a box and our answer follows.

Answer to the general comment:

> First, you improve the performances of your pervious work (Caseiro et al 2018) in detecting flaring sites, adding a temperature filtering.

We indeed complete our previous work with a filtering procedure which is based on the analysis of the temperature time series retrieved at the location of a given detection (the maximum temperature must be larger than 1500K) and on the persistence of the signal at that location (more than 5 quality detections per year).

> When you compare your results with VNF, you first use the 2012 VNF outputs (why not the 2017?) and then you take into account the combustion sources (https://ngdc.noaa.gov/eog/viirs/download_viirs_fire.html) identified by VNF instead of the flaring sites available at https://www.ngdc.noaa.gov/eog/viirs/download_global_flare.html for 2017 (the year of your analysis). I think it is a forcing applying the criteria developed in this work for SLSTR to select among the VNF combustion sources the flaring sites. The latter are directly provided by NOAA at https://www.ngdc.noaa.gov/eog/viirs/download_global_flare.html.

Our first decision was to use only published data for the activity and emissions comparisons and the most up-to-date VNF data for the characterisation (in our case, temperature), after applying a similar procedure as the one used in our work (i.e. gridding). We accept the suggestion and include the 2017 VNF temperature and activity data in our analysis. See section 3.5 for the comparison with the 2017 VNF dataset.

We now answer the section-specific suggestions/corrections:

> **Abstract**
>
> - We calculate the global flared gas volumes and black carbon emissions in 2017 by ~~(1)~~ applying (1) a previously developed hot spot detection and characterisation algorithm to all observations of the SLSTR instrument on-board the Copernicus 5 satellite Sentinel-3A ~~in 2017~~ and (2) ~~applying~~ newly developed filters for identifying gas flares and corrections for calculating both flared gas volumes (BCM) and black carbon emission (g/m^3) ~~estimates~~.
> - The comparison of our results with those of the VIIRS N~~-~~ightfire data set indicates a good fit between the two methods.
> - Please, remove the space at the beginning of the bracket (https://eccad3.sedoo.fr/#GFlaringS3, DOI 10.25326/19 (Caseiro and Kaiser, 2019))

All your recommendations were followed in the updated manuscript, except the units for the BC emissions, which we kept as mass (g).

Introduction

- Please, put the dot after the references: or convert the gas. (Rahimpour and Jokar, 2012; Emeka Ojijiagwo et al., 2016). This is the first case, I found many others in the paper.
- Improvements of flare gas recovery systems haves been recommended …
- GF also impacts the environment on a wider scale through the emission of pollutants and greenhouse gases like carbon dioxide (CO_2), carbon monoxide, black carbon (BC)…
- Of particular importance is also the ~~black carbon (~~BC~~)~~ emission emitted by GF. BC is a known carcinogen (Heinrich et al., 1994) as well as a short-lived climate forcer (IPCC, 2013). BC strongly a~~e~~ffects environments such …
- Satellite remote sensing has been utilized for regional and global identification and characterization of GF~~.~~ (Casadio et al., 2012b, a; Anejionu et al., 2014; Faruolo et al., 2014; Chowdhury et al., 2014; Anejionu et al., 2015; Faruolo et al., 2018). The most prominent system is NOAA's VIIRS (here add NOAA acronym Visible Infrared Imaging Radiometer Suite) Nightfire (VNF) dataset (see https://ngdc.noaa.gov/eog/viirs/download_viirs_fire.html), developed by Elvidge et al. (2013, 2016) for the detection and characterization of combustion sources ~~based on previous work (Elvidge et al., 2001, 2007, 2009, 2013)~~ and leading to a globally consistent survey of gas flaring volumes available extending back to 2012 (https://www.ngdc.noaa.gov/eog/viirs/download_global_flare.html).
- We recently published an adaptation and extension of the VNF~~VIIRS Nightfire~~ algorithm with which observations of the SLSTR ~~instrument~~ (Sea and Land Surface Temperature Radiometer) instrument on-board the Sentinel-3A satellite~~s~~ have~~can~~ been analysed~~, too~~ (Caseiro 30 et al., 2018).

- [last comment in the above box] Since the methodology is applicable to all (to date 2) the SLSTR instruments, we prefer to keep the reference to the Sentinel-3 satellites in the plural.
- All the other recommendations were followed in the updated manuscript.

- The main advantages of using our hot spot detection and characterisation algorithm lie in the ability to detect and quantify smaller flares and the foreseen long term data availability from the series of Sentinel-3 satellites in the Copernicus program. Additionally, SLSTR observations (night-time overpasses at 10:00 PM) complement those of VIIRS (1:30 AM) by filling observation gaps in the time series. I think the unique advantage your algorithm seems to offer, when compared to VNF, is its capability to identify smaller flares. Regarding the data continuity, also VIIRS is actually onboard two satellites (Suomi NPP and JPSS-1) and will also be flown on the JPSS-2 (launch in 2021), -3 (2026) and -4 (2031) satellite missions. You can rephrase this sentence, pointing out the potential of these algorithms, the possibility of integrating them as well as of continuously monitoring the phenomenon thanks to the long design life of satellite missions.
- Here, we describe a new dataset of global gas faring volume~~s~~ (BC~~D~~M) and BC emissions (g/m3), which we have derived from all Sentinel-3A SLSTR observations in 2017. In detail, c~~C~~hapter 2 describes newly developed methods for identifying gas flares among the observed hot sources, correcting for intermittent observations opportunities, and dynamically determining appropriate BC emission factors from the observations. The results ~~of applying the hot source detection and characteristion algorithm plus the newly developed methods to all SLSTR observations of 2017~~ are presented in Chapter 3, the~~. Finally, our~~ conclusions are summarised in Chapter 4.
- While in principle the methodology used is based on the ~~Nightfire algorithm developed for VIIRS~~VNF
- We already tested the method using oil and/or gas producing regions within a limited timespan and compared the results to the VNF~~VIIRS Nightfire~~

All your recommendations were followed in the updated manuscript, except the units for the BC emissions, which we kept as mass (g). Regarding the first comment of the box above, we have rephrased the idea focusing the complementarity of the instruments and the methods.

2.1 Hot spot detection and characterization
Figure 1 should be improved, explaining the GF filter.

2.2 Hot spot classification
2.2.1 Volcano filter

- The data were ~~as~~ filtered
- Many volcanoes do not consist of a single edifice, ~~but a volcanic field with~~ many individual eruptive fissures through which lava erupts may be present in a volcanic field~~.~~ (Siebert et al., 2010).

We have updated the manuscript following all these recommendations.

2.2.2 Discrimination of gas flares from other industrial hot sources
This paragraph is not completely clear. You are searching for a criterion to use for accurately detecting flaring sites. The starting point is your algorithm (Caseiro et al., 2018), to which you add a temperature filtering. I do not understand how you use the works of Elvidge et al. (2016) and Liu et al. (2018) in the definition of the temperature criterion. To this aim, you test several subsets. Can you explain what are these subsets? They are 8? They correspond the 8 columns in Table 1? Besides, I expected n_{Obs} was greater than n_{ObsHA}. Probably, it is more correct to use ≥ than >.

We have updated the caption of Table 1 with more detail:

Table 1. User's accuracy (UA, %) and commission error (C, %) of the hot spot discrimination strategies considered. n_{Obs} is the number of hot spot detections within a grid cell, n_{ObsHA} is the number of high-accuracy hot spot detections within a grid cell, T_{min} is the minimum temperature retrieved among all the hot spots detected within a grid cell, T_{max} is the maximum temperature retrieved among all the hot spots detected within a grid cell, n_{cells} is the number of grid cells that comply to the thresholds. In order to discriminate gas flares from other hot spots we discriminate hot spots based on their persistency (n_{Obs} and n_{ObsHA}) and on their temperature time series (T_{min} and T_{max}). We have tried 8 combinations (discrimination strategies) of thresholds on those variables. Each column represent a tested discrimination strategy. For each of the 8 combinations, we examine high-resolution imagery for 100 random onshore locations (800 in total) in order to verify the presence of a gas flare. The goal is to maximize user's accuracy (UA) and minimize commission error (C) while minimizing the omission error (here, the variation in n_{cells} is used as a proxy). The discrimination strategy #5 was selected as the most suitable.

combination	#1	#2	#3	#4	#5	#6	#7	#8
n_{Obs} >	–	3	4	–	–	–	–	–
n_{ObsHA} >	2	2	2	5	5	5	7	7
T_{min} (K) >	1000	1000	–	–	–	–	–	–
T_{max} (K) >	1400	1400	800	1200	1500	1800	1200	1500
n_{cells}	6733	5872	9469	6817	6232	5485	5527	5129
UA	84±6	86±8	60±10	77±13	85±11	88±10	73±14	87±11
C	7±3	4±2	19±11	6±4	3±1	1±1	8±5	2±1

In the text, we also give more detail in order to explain how we based our temperature considerations on the works of C. Elvidge and Y. Liu:

The temperature value used in the selection process of a discrimination strategy is based on Elvidge et al. (2016) and on the recent work by Liu et al. (2018), who derived gas flaring temperatures of 1000 K to 2600 K from the VIIRS Nightfire database, depending on the type of operation (shale oil or gas, offshore, onshore or refinery). Most of the gas flares display temperatures between 1650 K and 1850 K. However, temperatures can occasionally be as low as 1300 K. We therefore test for the minimum andor for the maximum temperature for all the high-accuracy detections within a grid cell (T_{min} and T_{max}, respectively). The temperature range reported by Elvidge et al. (2016) and Liu et al. (2018) overlaps with particularly hot detections from the coal chemical industry and steel plants. Therefore, additional criteria are needed for identifying gas flares in the hot source dataset.

In order to select the discriminating strategy we test several subsets of the gridded high-accuracy hot spot database. For each of the 8 subsets described in Table 1, a sample of 100 random onshore grid cells complying to the defined thresholds have been tested by examining high-resolution imagery (Google Earth) and the locations are classified into four categories:

2.3 Determination of flared volumes and black carbon emissions

- Please, explain the terms BCMmin, BCMmax, BCMbest in this order, to facilitate the comprehension.

This was updated as suggested.

- The emissions of black carbon (BC) from gas flares are estimated using reported emissions factors (EF). It could be useful to specify the formulation applied for their computation.

We have somewhat rearranged this paragraph and included a short introductory text to explain our approach:

The emissions of black carbon (BC) from gas flares are estimated using reported emissions factors (EF). Klimont et al. (2017) recognized the limited number of measurements of flaring emissions. Here, we attempt to consider the limited information available on the EF and maximize the use of the available information on the flare characteristics.

Schwarz et al. (2015) and Weyant et al. (2016) conducted field experiments in the Bakken formation (USA) and derived EFs of 0.57±0.14 $g.m^{-3}$ and 0.13±0.36 $g.m^{-3}$ (using the Single Particle Soot Photometer) or 0.28 $g.m^{-3}$ (using the Particle Soot Absorption Photometer), respectively. However, flared gas has not the same composition everywhere and Huang and Fu (2016) considered the regional variability of the EF. The authors applied the function which relates EF to the volumetric gas heating value derived in the laboratory by McEwen and Johnson (2012) to globally compiled gas composition data. Klimont et al. (2017) considered, for the Greenhouse Gas – Air Pollution Interactions and Synergies (GAINS) model, the EF derived by Schwarz et al. (2015) of 0.57 $g.m^{-3}$ for well-operated flares (i.e. Organisation for Economic Co-operation and Development (OECD) countries) and a maximum of 1.75 $g.m^{-3}$ for other countries. Stohl et al. (2013) used an EF of 1.6 $g.m^{-3}$ from a previous GAINS version. In the present work, we apply the same concept of a varying EF but use the flare temperature as an indication of the combustion completeness, instead of the country of origin as an indication of the flare operation. Flaring temperatures close to the adiabatic flame temperature for natural gas (around 2500 K) are associated with more complete combustion and therefore lower BC emissions. On the other hand, low flaring temperatures (700 K and below) are associated with higher BC emissions. Between the two extremes, the BC emission is scaled linearly as a function of the flaring temperature (see Figure 3). To the best of our knowledge, this is the first time that operating practices are taken into consideration when assigning the EF.

- GAINS: please, extend the acronym.

The acronym is explained in the text.

- You define flaring site a site with a temperature above 1500K. Why do you compute the EFs for lower temperatures?

The flaring site is defined as a grid cell for which the count of high-accuracy hot spots is larger than 5 and the maximum temperature is larger than 1500K. Although the maximum retrieved temperature must be larger than 1500K, temperature for individual high-accuracy hot spots within the grid cell may be lower than 1500K.

- With this methodology we estimate a wide range of possible activity (BCM) and BC emissions (g/m^3)

The recommendation was followed in the updated manuscript although the unit for the BC emissions was kept as mass (g).

- Can you better explain this sentence, please? I do not understand it: "We conservatively assume that this range of possibilities represents 6 × σ, and report the uncertainty of the best estimates as 1 × σ".

For clarity, we have removed this part from the paper and report the best estimate together with the range.

3. Results

3.1 Hot spots and flaring sites

I have concerns about this section. Your paper focuses on gas flaring, the previous one (Caseiro et al., 2018) on hotspots. For this reason, you can join Figures 4, 5, 6 using three colors for discriminating hotspots, high confidence hotspots and flaring sites. Besides, I do not understand why you compare the SLSTR globa detections for 2017 with the VNF in 2012. The VNF data for 2017 are available; you indeed use them in sectior 3.3.

Figures 4, 5 and 6 were merged into a single figure. Please see the resulting figure below.

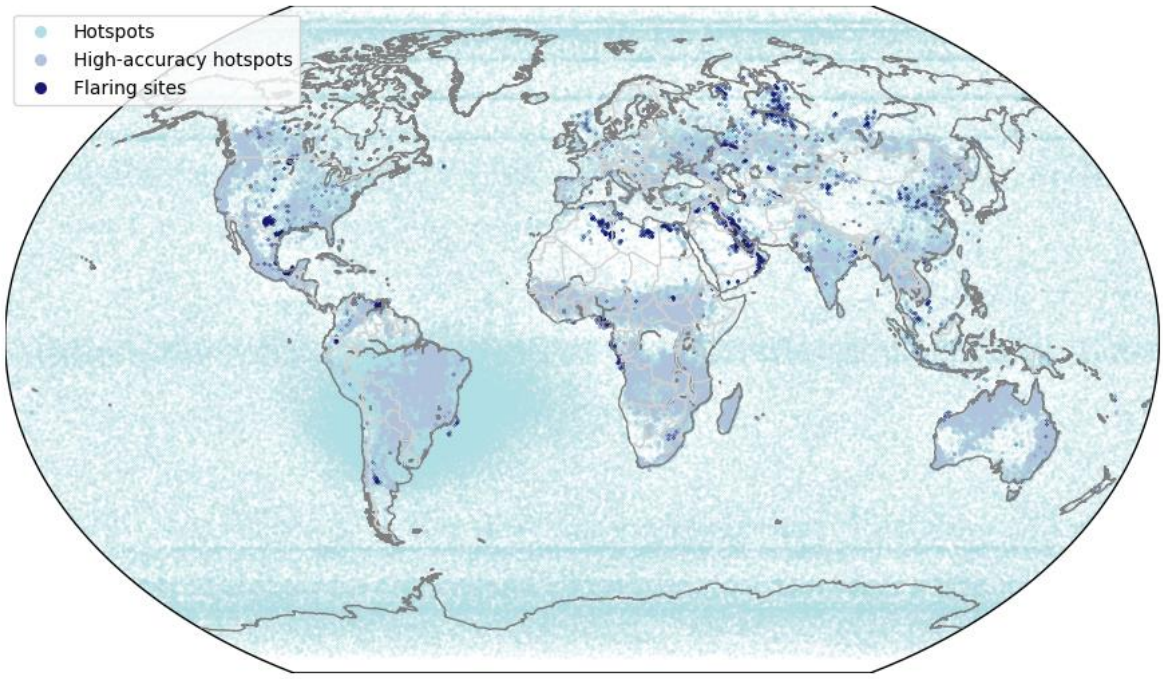

- Russia (985) and the United States (917) are the countries with the highest number of flaring locations (Figure 7).
- The time series of the cumulative number of the high accuracy observations for the most active flaring location (in Venezuela, see Section 3.4) is shown in Figure 8. It shows flaring activity throughout the year. In my opinion, it is not useful and interesting. Remove Figure 8.

These suggestions were followed.

I think 3.2 and 3.3 are subsections of 3.1: they become 3.1.1 and 3.1.2.

We feel that the three sections bring enough information individually to be treated as being at the same level: 3.1 deals with the detection itself, 3.2 with their characteristics and in 3.3 we derive the activity. To make this clear, the title of 3.1 has been updated: “Flaring locations”.

- Figures 10, 11 and 12 are not useful, in my opinion they could be removed. You can indeed add before Figure 9 and Figure 13, respectively, a global map (in color scale) showing the temperatures and RP values for the 6232 sites.

We have removed Figures 10, 11 and 12.

We have added figures for the global average T distribution:

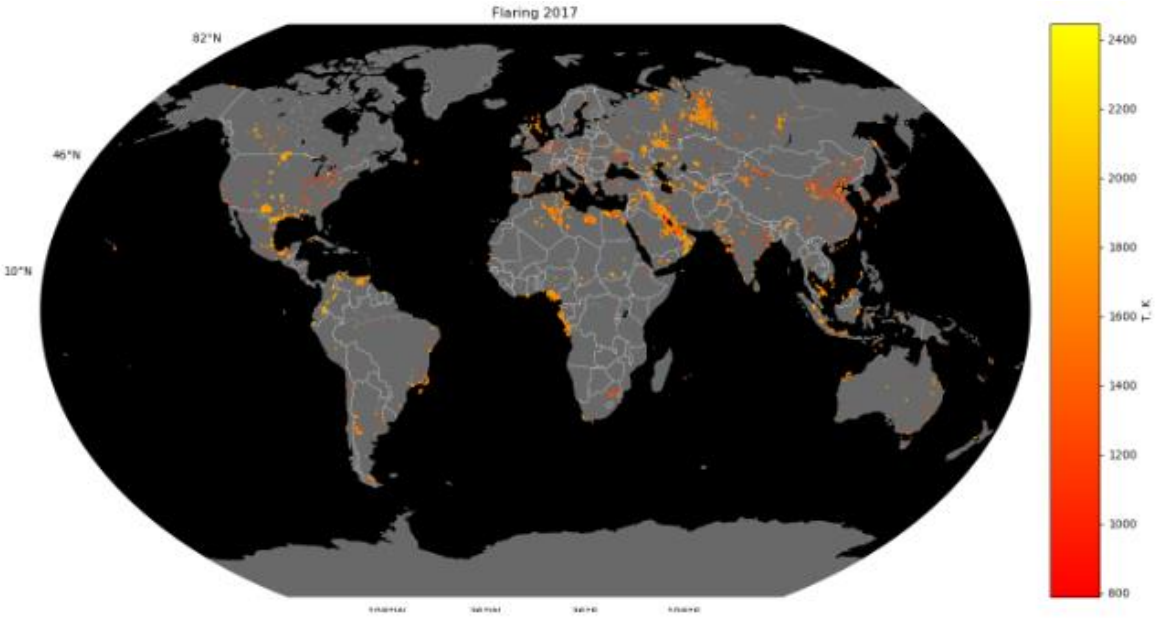

Figure 7. Average flaring temperature (K) at the 6232 flaring locations.

and similarly for RP:

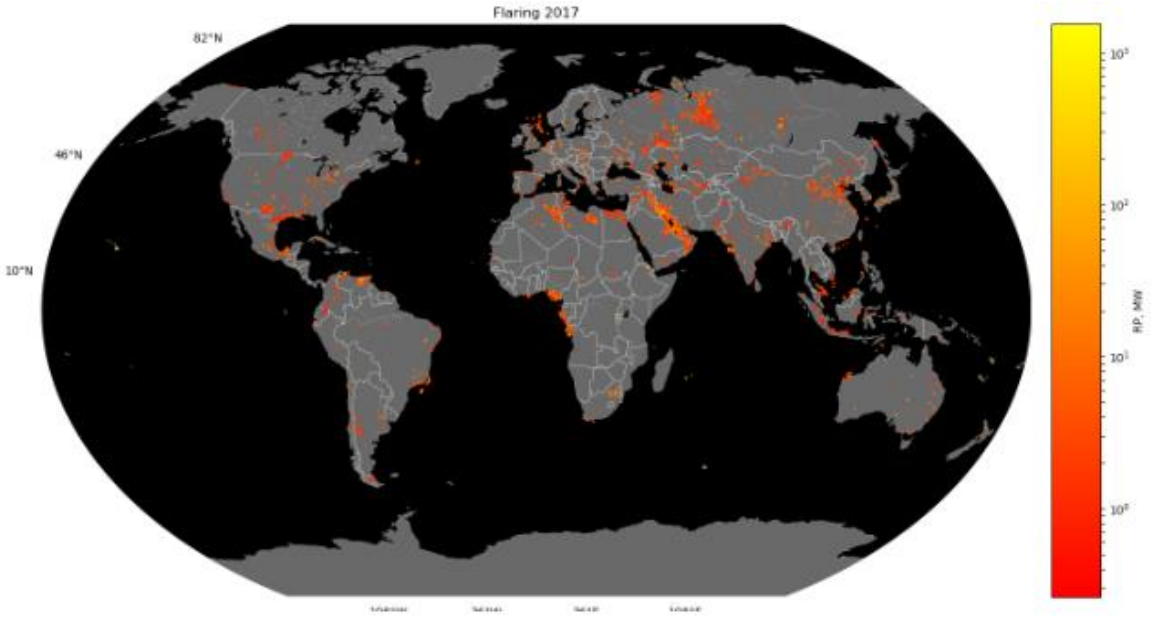

Figure 9. Average radiative power (MW) at the 6232 flaring locations.

- Figure 9. Distribution of the average retrieved ~~hot spot~~ temperature (K) for the flaring locations

The suggestion was followed.

- The average temperature at the flaring locations approximately ranges from 950 K to 2250 K. This is slightly lower than the range reported by Liu et al. (2018) (please, can you specify the values) who used VIIRS Nightfire data, as expected from our previous study (Caseiro et al., 2018). It confirms the bi-modal distribution with modes around 1750 K and 1200 K that is has also been observed by VIIRS.

The range given in Liu et al. (2018) was specified in the manuscript.

- The section "Comparison with VIIRS Nightfire" should be modified. As before explained, being the focus of your work the gas flaring, you should compare your results with the VNF flaring sites (available at https://www.ngdc.noaa.gov/eog/viirs/download_global_flare.html), avoiding to select these sites among the VNF combustion sources applying the criteria used for SLSTR.

The section was rewritten taking into consideration your suggestions. The section is now at the end of the "Results" chapter and we included a comparison of the activity (flared volumes) as well.

- You never cite Figure 14 in the paper. The figure is not useful, as figures 10-12.

Figure 14 was removed from the manuscript.

3.4 Flared volumes (new 3.2)
As before, you should use BCM data available at https://www.ngdc.noaa.gov/eog/viirs/download_global_flare.html for the comparison with your estimates in 2017. It would be interesting the map of the global distribution of BCMbest. In Figure 20 you could add the distribution derived by the VNF data elaboration.

3.5 BC emissions (new 3.3)
As for BCM, you can add a global map of BC emissions.

This section was reworked also following the recommendations from the other reviewer and the short comments. It now includes VNF data from 2017 as suggested. Please see the updated manuscript.

Conclusions
To reorganize based on new suggested analyses. In any case:

This section was reworked also following the recommendations from the other reviewer and the short comments. Please see the updated manuscript.

- The sentence "We present a new gas flaring discrimination procedure, based on two characteristics of gas flares: persistence and temperature" is not correct. This procedure is not new, being the one most used to identify gas flares. Respect to your methodology, you simply add a temperature filtering to improve the detection of flaring sites.

We have updated this sentence of the conclusions: "We adapt the procedure most commonly used to discriminate gas flares (based on two characteristics of gas flares: persistence and temperature) to our specific hotspot detection methodology."

- "Additionally to the detection we present a way to assess the volume of flared gas": is not true. You apply a widely declared model developed by Elvidge et al (2016) to compute monthly flared volumes, adding a scaling factor, which takes into account the operation time of the sites.

We have reworded the first two sentences of this paragraph: "Additionally to the detection we assess the volume of flared gas based on the observed relationship between the flared volume and observed flare radiative energy."

Dear reviewer,

In this document, your original comments are framed by a box and our answer follows.

1. The methodology section is too brief and the reader needs to go through many other publications to gain even an overview of the current one. This is inconvenient for the general readers. E.g. in line 12 of page 3, instead of directly pointing to Caserio et al. (2018), just very briefly give an overview of the salient features of the algorithm.

Similarly, for line 19 of page 3, explain why analyzing he cluster of contiguous hot pixels advantageous than the spatial maxima method. Additionally, what could be the disadvantages of this method and how are they taken care of: e.g. What are the possibilities that pixels representing different intensities taken as an average may lead to an overall over or underestimation for a grid or lead to a mixing of two very different signals.

We have added several sentences in the beginning of the methodology section. However, since the methodology has already been published and this paper is intended to describe a dataset, we preferred to keep comments on the methodology short in order to keep the focus of the reader on the data.

2. Section 2.2.2 : state the background, advantages and disadvantages for using the Equations 1 and 2.

Equation 1, user's accuracy: The User's Accuracy is the accuracy from the point of view of a map user. This metrics represents the frequency with which a class on the map corresponds to the ground truth. In our case, the User's accuracy is quantified between at least the verified flaring locations and at most the sum of the verified and the likely flaring locations.

Equation 2, commission error: Commission errors are calculated by reviewing the classified sites for incorrect classifications. In the present work, the commission error is quantified between at least the locations without any industry or infrastructure and at most the sum of the locations without any industry or infrastructure and the unlikely flaring locations.

We have updated the manuscript accordingly.

3. Section 2.3: The BC estimation formula seems too oversimplified. E.g. equation 4 does not take into account the different flares leading to different amounts of BC emissions over the year. This may be a reason leading to underestimation w.r.t. other inventories: I believe authors should instead try something like a weighted average or a more representative method to arrive at a better estimate.

The BC emission factor takes into account the different state of a flare in terms of burning efficiency in that it is determined as a function of temperature (please refer to Figure 3). While appearing to be simple, we argue that this methodology goes beyond differentiating between static flare types by parameterising the underlying physical reason (flare temperature resp. burning efficiency). It is therefore able to account for different and varying emission factors. Equation 4 is used to compute the total activity or emission of a flaring site. We agree that the estimation of the number days of operation for each flaring site is the part of the entire method with the most assumptions and thus

the largest potential source of errors. However, we consider it to be a valid approach when only detections of hot spots are available as input. Please refer to our answer to the corresponding comments by Chris Elvidge for more details.

4. The diagrams need to be more complete by themselves e.g. y label missing in fig 11, 12 (only writing it within caption is not sufficient), cbar label missing in fig 10

Figure 10, 11 and 12 were removed from the manuscript following the recommendation by the other anonymous reviewer.

Page 2 Line 11: Contributions to what e.g. CO2 equivalent?
Page 2 Line 14: Replace ‘emitted’ by ‘from’
Page 3 Line 4: Replace ‘chapter’ by ‘section’
Page 21 line 9: what is Upstram?
Page 24 Line 4: Replace ‘allow’ by ‘allows’

The Upstream oil and gas industry is that part of the oil and gas industry which includes searching for potential underground or underwater crude oil and natural gas fields, drilling exploratory wells, and subsequently drilling and operating the wells that recover and bring the crude oil or raw natural gas to the surface. An addition was made to the text.

All the other recommendations were followed.

Dear Chris Elvidge, thank you very much for your valuable and constructive comments. We have followed most of your suggestions and we find that our paper is now generally improved.

In this document, your original comments are framed by a box and our answer follows.

Review of "Gas flaring activity and black carbon emissions in 2017 derived from Sentinel-3A SLSTR" The paper attempts to locate all the active gas flares of 2017 and estimate their flare gas volumes using nighttime data collected by the Sea and Land Surface Temperature Radiometer (SLSTR) instrument flown on-board the Copernicus satellite Sentinel-3A. The basic detection algorithm for the individual nights of data follows the VIIRS nightfire (VNF) method and appears to be solid. But the steps used to go from the individual nights of data to the annual summary are questionable and should be revisited.

1. The SLSTR results found 6232 flaring sites in 2017. This compares to over 10,000 flares reported by the VIIRS nightfire team for 2017 (https://eogdata.mines.edu/download_global_flare.html).

The section on the comparison with VIIRS Nightfire has been totally rewritten and is now at the end of the Results chapter. We now compare our results to the gridded detections and activity data for 2017 provided by the VIIRS Nightfire team.

We argue that both methodologies globally agree, in that they capture roughly the same flaring regions around the world. However, a closer look reveals that those regions are more populated by the VIIRS Nightfire results than by our own. We trace back that behaviour to small geolocation inaccuracies, the clustering of hot pixels in our algorithm (against the analysis of local maxima) and the VIIRS larger swath which provides more opportunities to detect a flaring site. We attempt to quantify the contribution of these factors to the observed difference in terms of flaring locations between both methodologies. Of the 10185 flaring locations produced by the gridding of the VNF data, 2964 are coincident with the flaring locations presented here, 1507 are adjacent and 1651 are less than 4 grid cells away, which can be interpreted as due to geolocation inaccuracies and the clustering of hot pixels. Finally, 4063 are "distant", i.e. more than 4 grid cells away from the closest SLSTR flaring location. A closer analysis reveals that our methodology also captures activity at those locations, though not enough to be classified as flaring following our criteria. This indicates a low activity and, indeed, the associated BCM in the VNF record is low (8.67 BCM, a few percent of the global total of 151 BCM).

In summary, we attribute different flaring locations in the datasets as follows:

- Adjacent (7.3 BCM in VNF): a mix of geolocation error and clustering
- A distance from adjacent up to 4 grid cells (3.1 BCM in VNF): a mix of clustering and intermittent operation
- Larger distances (8.7 BCM in VNF): intermittent operation and more detection opportunities by VIIRS due to larger swath.

2. Many flares are intermittent. The nightly flare detection data does not contain sufficient information to account cloud and solar contamination effects that could effect the annual flared gas volume calculation. Hence the annual characterization of flared gas volume should calculate the "duty cycle" or "percent frequency of detection" for each flaring site. The VNF team makes the calculation based on flare detection numbers in the set of nighttime cloud-free observations made of the site during the year. Because the nightly VNF product only contains the detections – the annual analysis includes an

inventory of the cloud state (cloudy or clear) for the nights lacking VNF collection that are free of solar contamination. The VNF method excludes both sunlit and cloudy observations in the calculation of flaring site duty cycle. The method reported in this paper (section 2.3 and Figure 2) is woefully inadequate and appears to have resulted in a drastic underestimation of annual flared gas volume in Russia. I suspect that the method in Figure 2 does not account for solar contamination outages during summer months – as shown below with VNF for a flare in northern Siberia.

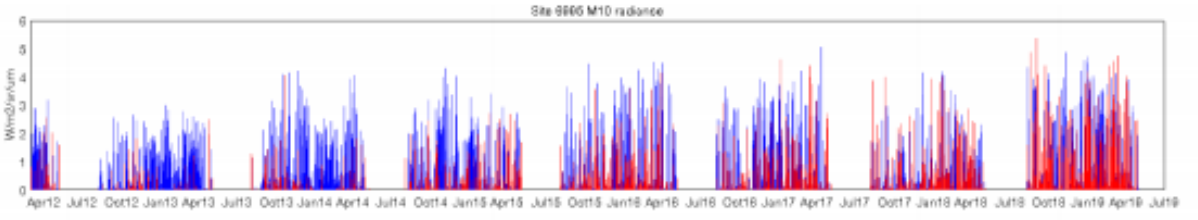

Fig. 1. Temporal profile VNF SWIR radiance for a flare in Siberia. Each year there is an outage period due to solar contamination.

We acknowledge that the method for correcting for variable observation opportunity is less sophisticated than the one employed in VNF. It should, however, be capable of partly correcting the effect partial and complete solar contamination. The underlying assumption is that SLSTR happened to observe a few gas flaring locations in mostly cloud-free condition during 2017. With almost continuous operation, these should be the locations with the largest numbers of detections. In this case, the numbers of detections are also estimates for the numbers of detection opportunities, including the effects of number of satellite overpasses and solar contamination. The number of satellite overpass times increases for higher latitudes; this should increase this largest number of detections for higher latitudes. On the other hand, the summer period during which more observations are contaminated with solar radiation is longer for higher latitudes. This has the opposite effect of reducing the largest number of detections for higher latitude. The latter effect appears to be stronger, given the behaviour depicted in Fig. 2. An additional error occurs due to the variability in average percentage of cloud cover, which the presented method approximates to be constant zonally and to vary smoothly meridionally. Therefore, the method is considered to be applicable with less effort but also less accuracy than a detailed recording of the detection opportunities for each flaring site. In particular, this method should improve the results when only information on hot spot detections but not on detection opportunity is available.

3. The paper lacks detail on the method used to discriminate clear versus cloudy observations. In addition, the paper makes several assertions that should be rechecked.

The discrimination of clear versus cloudy observations is performed based on the cloud mask in the SLSTR L1b product during the hot spot detection procedure, which is described in our earlier paper and simply applied in this one. We agree that a second processing of the SLSTR L1b products to calculate the detection opportunities for each flaring site based on its individual solar and cloud contamination would be a more accurate process. However, due to budget (the project has been over for more than 2 years now) and time (the main authors of the study are now in new positions) constraints, it is not possible for the authors to conduct this now. It should certainly be considered for possible further developments of the methodology.

4. The paper makes several claims that the “SLSTR-based methodology is able to detect smaller gas flares”. No evidence is presented to back up this claim.

The claim was based on the night-time availability of a second SWIR channel. The statement was completed in the manuscript (see the answer to the next comment).

5. The paper state that the VNF product only uses a single shortwave infrared channel. This was the case for early VNF data. However, from January 2018 forward VNF from two satellites has included two SWIR bands.

We have updated the information in our manuscript (section 2.1 Hot spot detection and characterization): [referring to the comparison conducted in our previous paper] The results showed a good agreement of our hot source detection when investigating persistent hot spots with the advantage of the Sentinel-3A's SLSTR algorithm in detecting and quantifying smaller flares, due to the night-time availability of a second SWIR channel. Although this was the case at the time of writing our previous paper, from January 2018 VIIRS Nightfire uses two SWIR channels at night and the detections are conducted by two VIIRS instruments.

The reference to the outdated feature was removed from the end of the introduction.

My recommendation is that the paper undergo major revision and a second round of peer review prior to publication. The authors should make a specific comparison against the VNF product from 2017 to better understand difference between the SLSTR and VIIRS flaring sites and flared gas volumes. Are there specific geographic regions where one system detects more flares or more flared gas volumes? Since the instruments and detection algorithms are so similar, the authors should figure out the reason behind the discrepancies. To make a direct comparison of the combustion source detection limits with VNF, the authors can follow the methods outlined in https://www.mdpi.com/2072-4292/11/4/395

This crosschecking with VNF could lead to major improvements in the gas flaring results from SLSTR and a far better paper.

We have considerably revised our paper and have added several new analysis and figures to better illustrate the results of our work. In particular, we have added a comparison the VNF product from 2017 as recommended. The suggested further analysis along the lines of the paper recommended by the reviewer would certainly be worthwhile but is considered to be somewhat out of the scope of the present submission. In the Elvidge *et al.* 2019 paper, the authors analyze the hotspots retrieved using not only a SWIR channel as primary detection, but also a MWIR channel. In our present work, we focus on the detections achieved using the SWIR as primary channel.

Dear Daniel Fisher,

Thank you very much for your valuable comments. We have followed your suggestions and we find that our paper is now improved in general and more thoroughly compared with the most recent literature on the subject.

In this document, your original comments are framed by a box and our answer follows.

In this paper the thermal anomaly detection and characterisation algorithm developed in Casiero et al. (2018), based on NightFire, is applied to Sentinel-3 SLSTR data with the objective of evaluating global gas flaring radiant heat output and the associated estimates of black carbon emissions. The resulting thermal anomaly outputs, generated for 2017, are subjected to various filters to partition flaring and non-flaring anomalies, with the most crucial step being the application of a persistency test of more than five observations in the 12 month evaluation period in addition to a minimum temperature limit of 1500 K, which must be exceeded. A normalisation process is then applied to the detected gas flaring sites to account for differences in sampling opportunities to generate an adjusted measure of radiant heat output for each flaring site. Black carbon emissions estimates are then generated from the adjusted radiant heat estimates using appropriate emission factors. Finally comparison against various other datasets are made to assess the validity of the SLSTR generated datasets.

Whilst in general the paper is reasonably well written, there is a potentially significant flaw in the gas flare characterisation approach which must be investigated and addressed before publication can be recommended. In Elvidge et al. (2016) and Fisher et al. (2019) it is demonstrated that a substantial proportion of global gas flaring radiant heat output arises from a small subset of flaring sites global (50% of output comes from 5-10% of all flares). Some of these flares are extremely radiant such as the Punta de Mata site in Venezuela identified by the authors (and elsewhere), and they attribute 0.623 BCM of flared gas to this site in 2017. In comparison, Elvidge et al (2016) identified that 1.13 BCM of gas was flared at this site in 2012. The discrepancy between these two values is concerning, particularly as Venezuela has been shown to have had a very large increase in gas flare radiant heat output since 2012 (Fisher et al., 2019), and given the characteristics of gas flaring (e.g. most radiant heat being produced by a small subset of sites) one would expect that the most active flaring site in Venezuela to have show at least some increase, and not the reported decrease.

I think that this result may be arising from a potential issue with the channels used by the algorithm. In Elvidge et al. (2019) the issue of saturation in the (M11) 2.2 m and (M12) 3.7 m VIIRS channels is identified and I would expect that a similar issue is occurring with SLSTR, particularly given the enhancement in pixel resolution from 750 m2 to 500 m2. The channels employed in the Casiero et al. (2018) for the estimation of gas flare radiant heat output are S5 (1.6 μm), S6 (2.2 μm) and S7/F1 (3.7 μm). Given its specifications, the S7 channel likely saturates on a regular basis over gas flares, and this is identified, as is the potential for using the F1 channel when this occurs. However, no assessment of the

saturation characteristics of the SWIR channels is made, and whilst the S5 channel likely does not saturate, the same cannot be said for the S6 channel. Furthermore, being a relatively new instrument the performance of the F1 channel has not been evaluated, and it needs to be demonstrated that it reaches the specified dynamic range performance levels (the same can be said for the SWIR channels). If any of the channels are saturating then the effects on the retrieved radiant heat can be significant as shown in Elvidge et al. (2019), and in the current configuration of the algorithm used in this paper these saturation events may well be being missed. I expect, given that a significant proportion of radiant heat output arises from a subset of highly radiant flaring sites, the impact of saturation on the reported global total of radiant heat output and in turn BCM could well be significant and must be explored.

To do so I would recommend:

(1) evaluating the Planck curves of the most radiant flare sites identified globally and check the deviations of the various spectral observations from the curves that might indicate saturation of specific channels, giving at least an indication of saturation effects on SLSTR.

We already address the reviewer's concern of S7 and S9 saturation by using F1 and F2 when necessary (see also Caseiro et al. 2018). Saturation of the SWIR channels do not lead to a good fit and do not converge. Please find all the Planck curve fits within the most active flaring location at the end of this document.

(2) I would recommend applying the single channel radiant heat estimation approach of Fisher and Wooster (2018) developed in part for application to the S5 channel of the SLSTR sensor and see if any significant differences are observed, this would be a very straightforward comparison.

We added a new subsection where we apply the single SWIR method (Fisher and Wooster 2018 and 2019) to our detections and compare the results in terms of radiative power (RP), see figure below. We also compare our results with the results from Fisher and Wooster 2019. This shows that our method is biased high compared to the SWIR method and also gives larger maximum FRP values. Therefore, the FRP calculation should not lead to a low bias for the largest gas flares as suspected by the reviewer.

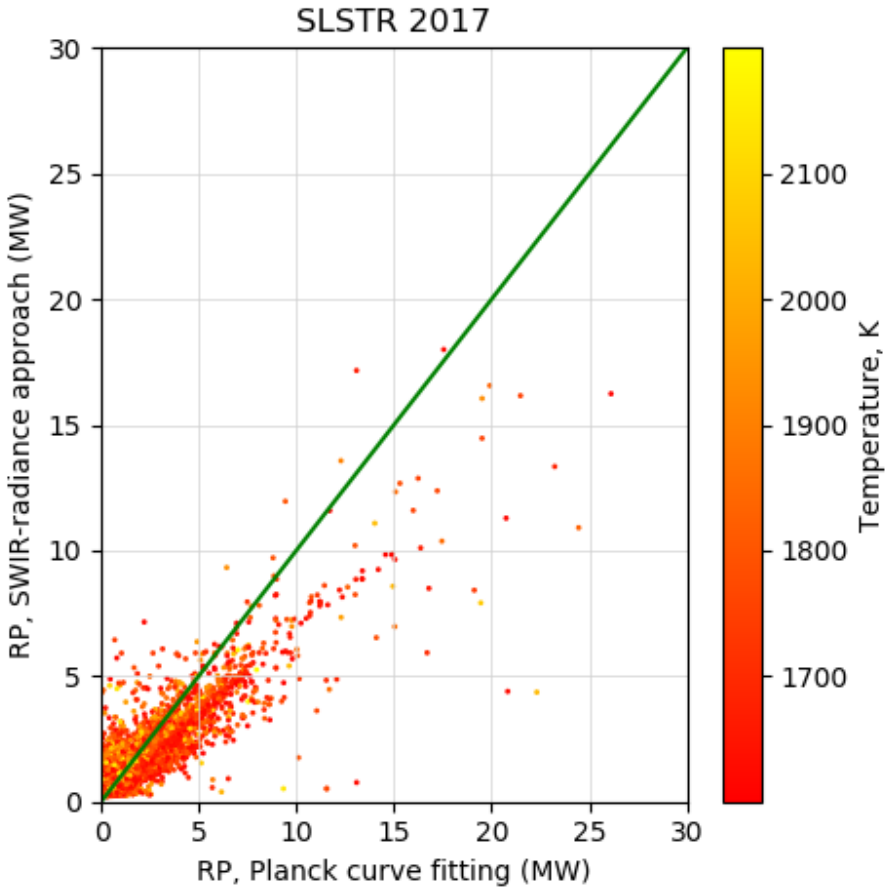

(3) I would then suggest that if a discrepancy for these larger flaring sites is found that the S3 channel is included as an additional constraint for these very large flares to try and improve the radiant heat estimates.

The NIR channels S3 (0.865 µm) and/or S4 (1.375 µm) are strong candidates to constrain more precisely the dual Planck curve fit. Both these channels are turned off at night, but during the commissioning phase of the satellite, which corresponded to the development phase of our methodology, they were switched on at night by ESA for a limited time period. Our conclusions were that the signal-to-noise ratio was too low for extracting additional information.

(4) It would be likely be useful to compare also against flare counts from Fig. 7 in Fisher and Wooster (2019) in addition to the NightFire comparison.

This has been added to the manuscript, see answer to recommendation #2.

Lastly, some key references are missing from the paper and should be included:

Anejionu, O.C., 2019. Rationale, historical developments and advances in remote sensing of gas flares. International Journal of Remote Sensing, 40(17), pp.6700-6719.

Elvidge, C.D., Zhizhin, M., Baugh, K., Hsu, F.C. and Ghosh, T., 2019. Extending nighttime combustion source detection limits with short wavelength VIIRS data. Remote Sensing, 11(4), p.395.

Fisher, D. and Wooster, M., 2018. Shortwave IR Adaption of the Mid-Infrared Radiance Method of Fire Radiative Power (FRP) Retrieval for Assessing Industrial Gas Flaring Output. Remote Sensing, 10(2), p.305.

Fisher, D. and Wooster, M.J., 2019. Multi-decade global gas flaring change inventoried using the ATSR-1, ATSR-2, AATSR and SLSTR data records. Remote Sensing of Environment, 232, p.111298.

1 + 2 + 4 were not originally included because they came out after or towards the end of the time of writing. All four are now cited in the paper.

Other references referred to here:

Caseiro, A., Rücker, G., Tiemann, J., Leimbach, D., Lorenz, E., Frauenberger, O. and Kaiser, J., 2018. Persistent Hot Spot Detection and Characterisation Using SLSTR. Remote Sensing, 10(7), p.1118.

Elvidge, C. D., Zhizhin, M., Baugh, K., Hsu, F.-C., and Ghosh, T.: Methods for Global Survey of Natural Gas Flaring from Visible Infrared Imaging Radiometer Suite Data, Energies, 9, 14,

Planck curve fits at the most active flaring location:

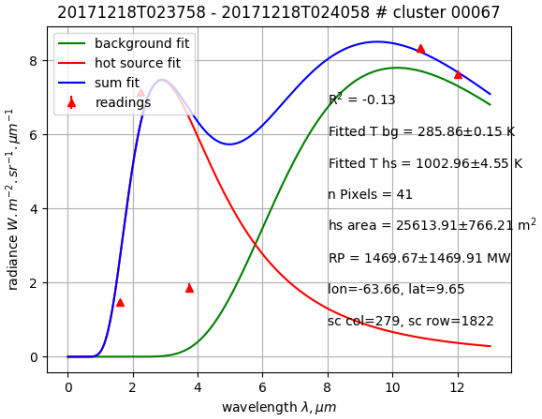

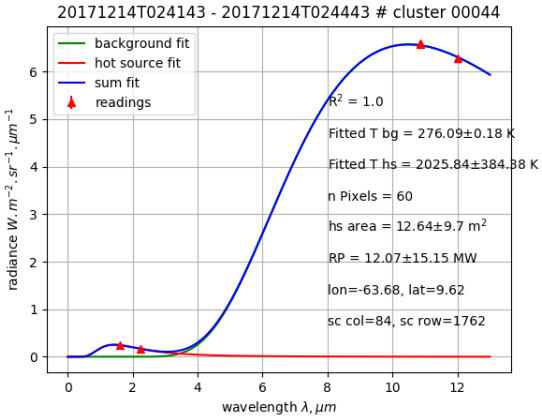

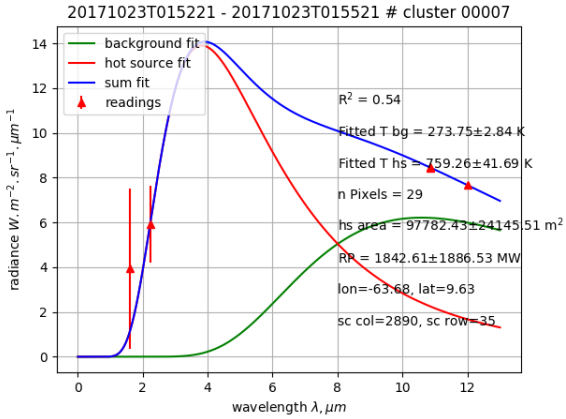

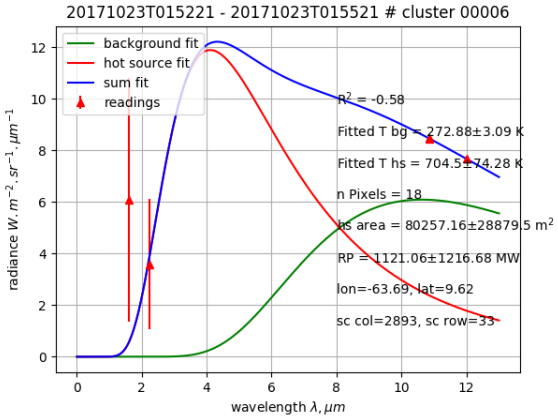

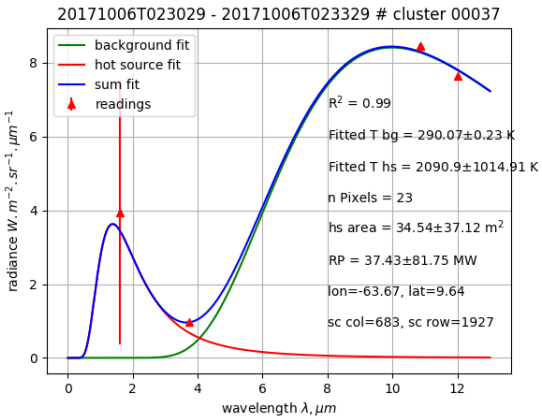

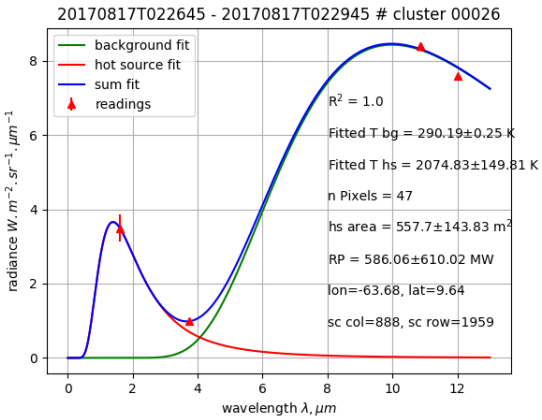

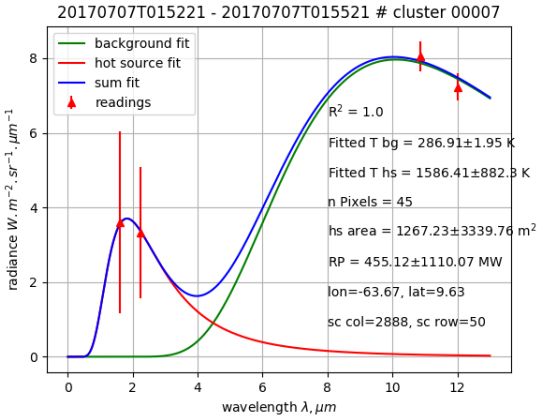
20170707T015221 - 20170707T015521 # cluster 00007
background fit
hot source fit
sum fit
readings
R² = 1.0
Fitted T bg = 286.91±1.95 K
Fitted T hs = 1586.41±882.3 K
n Pixels = 45
hs area = 1267.23±3339.76 m²
RP = 455.12±1110.07 MW
lon=-63.67, lat=9.63
sc col=2888, sc row=50
radiance W.m⁻².sr⁻¹.μm⁻¹
wavelength λ, μm

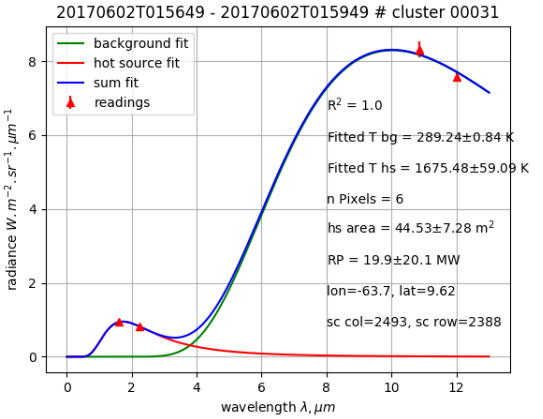
20170602T015649 - 20170602T015949 # cluster 00031
background fit
hot source fit
sum fit
readings
R² = 1.0
Fitted T bg = 289.24±0.84 K
Fitted T hs = 1675.48±59.09 K
n Pixels = 6
hs area = 44.53±7.28 m²
RP = 19.9±20.1 MW
lon=-63.7, lat=9.62
sc col=2493, sc row=2388
radiance W.m⁻².sr⁻¹.μm⁻¹
wavelength λ, μm

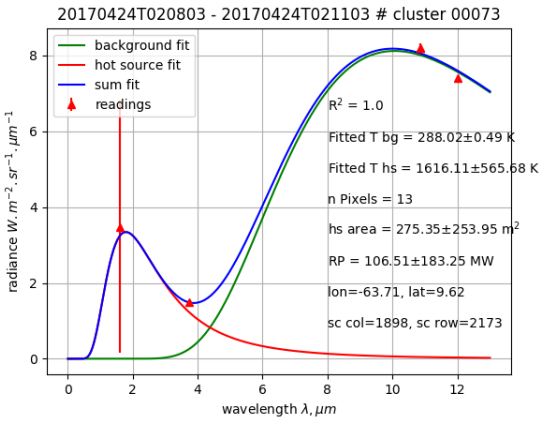
20170424T020803 - 20170424T021103 # cluster 00073
background fit
hot source fit
sum fit
readings
R² = 1.0
Fitted T bg = 288.02±0.49 K
Fitted T hs = 1616.11±565.68 K
n Pixels = 13
hs area = 275.35±253.95 m²
RP = 106.51±183.25 MW
lon=-63.71, lat=9.62
sc col=1898, sc row=2173
radiance W.m⁻².sr⁻¹.μm⁻¹
wavelength λ, μm

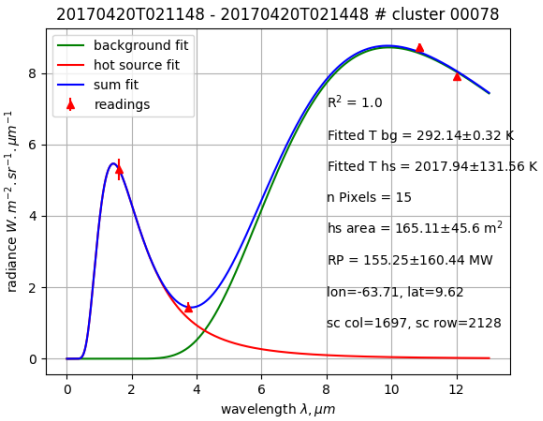
20170420T021148 - 20170420T021448 # cluster 00078
background fit
hot source fit
sum fit
readings
R² = 1.0
Fitted T bg = 292.14±0.32 K
Fitted T hs = 2017.94±131.56 K
n Pixels = 15
hs area = 165.11±45.6 m²
RP = 155.25±160.44 MW
lon=-63.71, lat=9.62
sc col=1697, sc row=2128
radiance W.m⁻².sr⁻¹.μm⁻¹
wavelength λ, μm

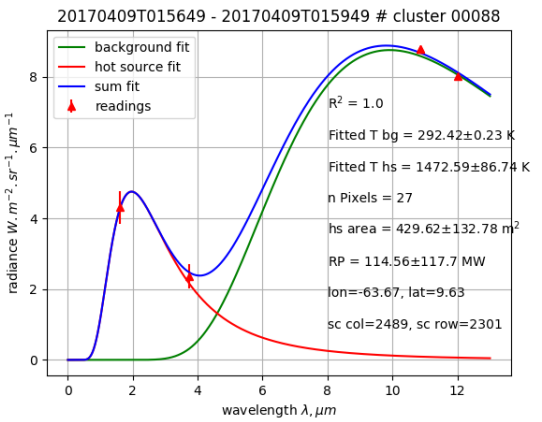
20170409T015649 - 20170409T015949 # cluster 00088
background fit
hot source fit
sum fit
readings
R² = 1.0
Fitted T bg = 292.42±0.23 K
Fitted T hs = 1472.59±86.74 K
n Pixels = 27
hs area = 429.62±132.78 m²
RP = 114.56±117.7 MW
lon=-63.67, lat=9.63
sc col=2489, sc row=2301
radiance W.m⁻².sr⁻¹.μm⁻¹
wavelength λ, μm

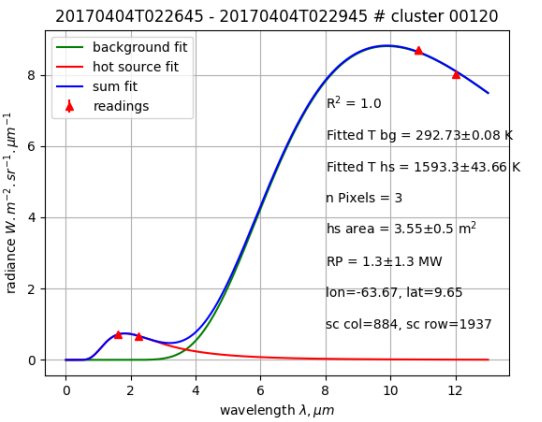
20170404T022645 - 20170404T022945 # cluster 00120
background fit
hot source fit
sum fit
readings
R² = 1.0
Fitted T bg = 292.73±0.08 K
Fitted T hs = 1593.3±43.66 K
n Pixels = 3
hs area = 3.55±0.5 m²
RP = 1.3±1.3 MW
lon=-63.67, lat=9.65
sc col=884, sc row=1937
radiance W.m⁻².sr⁻¹.μm⁻¹
wavelength λ, μm

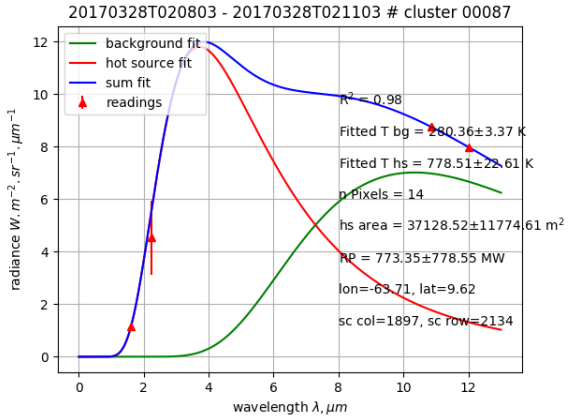
20170328T020803 - 20170328T021103 # cluster 00087
background fit
hot source fit
sum fit
readings
R^2 = 0.98
Fitted T bg = 280.36±3.37 K
Fitted T hs = 778.51±22.61 K
n Pixels = 14
hs area = 37128.52±11774.61 m^2
RP = 773.35±778.55 MW
lon=-63.71, lat=9.62
sc col=1897, sc row=2134
radiance $W.m^{-2}.sr^{-1}.\mu m^{-1}$
wavelength $\lambda, \mu m$

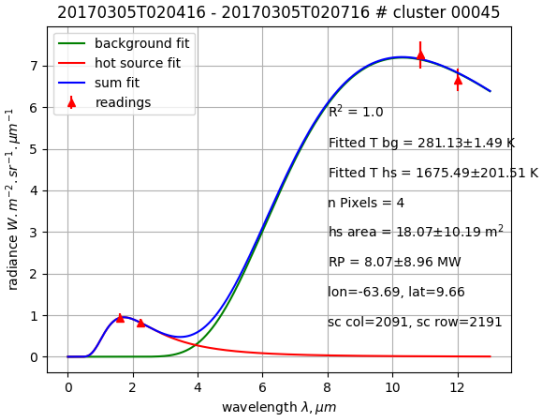
20170305T020416 - 20170305T020716 # cluster 00045
background fit
hot source fit
sum fit
readings
R^2 = 1.0
Fitted T bg = 281.13±1.49 K
Fitted T hs = 1675.49±201.51 K
n Pixels = 4
hs area = 18.07±10.19 m^2
RP = 8.07±8.96 MW
lon=-63.69, lat=9.66
sc col=2091, sc row=2191
radiance $W.m^{-2}.sr^{-1}.\mu m^{-1}$
wavelength $\lambda, \mu m$

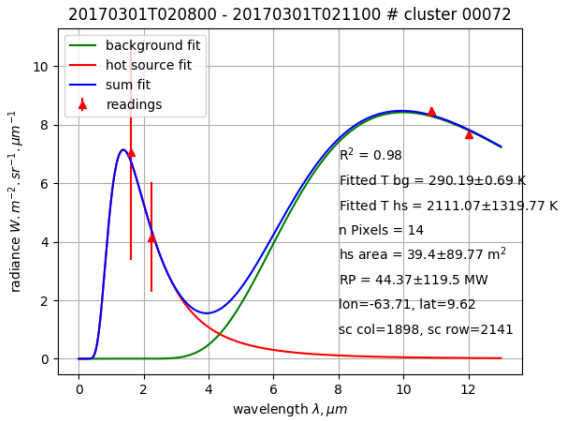
20170301T020800 - 20170301T021100 # cluster 00072
background fit
hot source fit
sum fit
readings
R^2 = 0.98
Fitted T bg = 290.19±0.69 K
Fitted T hs = 2111.07±1319.77 K
n Pixels = 14
hs area = 39.4±89.77 m^2
RP = 44.37±119.5 MW
lon=-63.71, lat=9.62
sc col=1898, sc row=2141
radiance $W.m^{-2}.sr^{-1}.\mu m^{-1}$
wavelength $\lambda, \mu m$

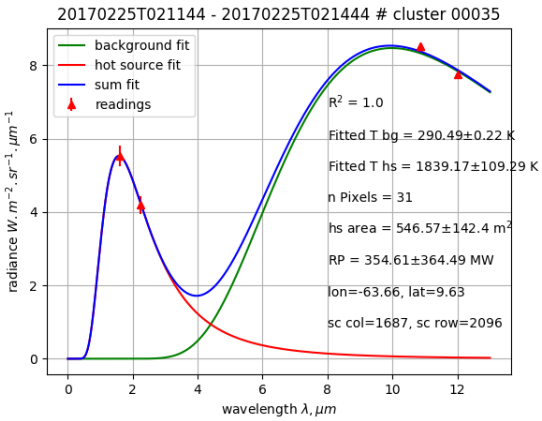
20170225T021144 - 20170225T021444 # cluster 00035
background fit
hot source fit
sum fit
readings
R^2 = 1.0
Fitted T bg = 290.49±0.22 K
Fitted T hs = 1839.17±109.29 K
n Pixels = 31
hs area = 546.57±142.4 m^2
RP = 354.61±364.49 MW
lon=-63.66, lat=9.63
sc col=1687, sc row=2096
radiance $W.m^{-2}.sr^{-1}.\mu m^{-1}$
wavelength $\lambda, \mu m$

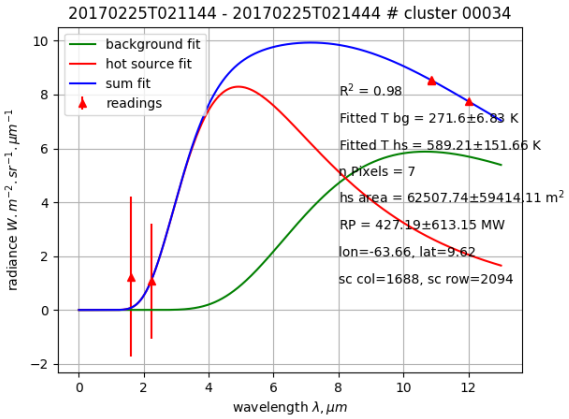
20170225T021144 - 20170225T021444 # cluster 00034
background fit
hot source fit
sum fit
readings
R^2 = 0.98
Fitted T bg = 271.6±6.83 K
Fitted T hs = 589.21±151.66 K
n Pixels = 7
hs area = 62507.74±59414.11 m^2
RP = 427.19±613.15 MW
lon=-63.66, lat=9.62
sc col=1688, sc row=2094
radiance $W.m^{-2}.sr^{-1}.\mu m^{-1}$
wavelength $\lambda, \mu m$

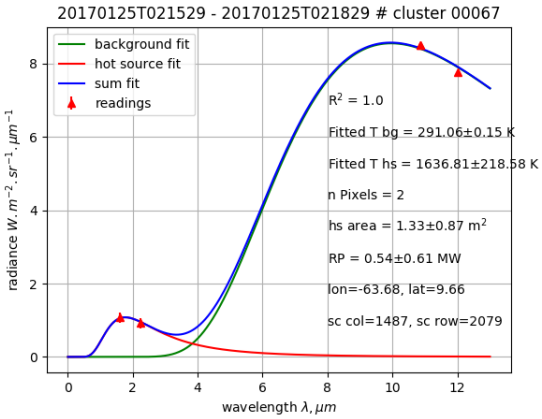
20170125T021529 - 20170125T021829 # cluster 00067
background fit
hot source fit
sum fit
readings
R^2 = 1.0
Fitted T bg = 291.06±0.15 K
Fitted T hs = 1636.81±218.58 K
n Pixels = 2
hs area = 1.33±0.87 m^2
RP = 0.54±0.61 MW
lon=-63.68, lat=9.66
sc col=1487, sc row=2079
radiance $W.m^{-2}.sr^{-1}.\mu m^{-1}$
wavelength $\lambda, \mu m$

https://doi.org/10.5194/essd-2019-99
Preprint. Discussion started: 25 July 2019

Open Access Earth System Science Data Discussions

Gas flaring activity and black carbon emissions in 2017 derived from Sentinel-3A SLSTR

Alexandre Caseiro[1], Berit Gehrke[1], Gernot Rücker[2], David Leimbach[2], and Johannes W. Kaiser[1,3]

[1]Max Planck Institute for Chemistry, Mainz, Germany
[2]Zebris GbR, Munich, Germany
[3]Deutscher Wetterdienst, Offenbach, Germany

Correspondence: Alexandre Caseiro (alexandre.caseiro@mpic.de)

Abstract. Gas flares are a regionally and globally significant source of atmospheric pollutants. They can be detected by satellite remote sensing. We calculate the global flared gas volume and black carbon emissions in 2017 by (1) applying a previously developed hot spot detection and characterisation algorithm to all observations of the Sea and Land Surface Temperature Radiometer (SLSTR) instrument on-board the Copernicus satellite Sentinel-3A in 2017 and (2) applying newly developed filters for identifying gas flares and corrections for calculating flared gas volumes (Billion Cubic Meters, BCM) and black carbon emission estimates. The filter to discriminate gas flares from other hot spots combines the unique flaring characteristics in terms of persistence and temperature. The comparison of our results with those of the Visible Infrared Imaging Radiometer Suite (VIIRS) nightfire data set indicates a good fit between the two methods. The calculation of black carbon emissions using our gas flaring data set and published emission factors show good agreement with recently published black carbon inventories. The data presented here can therefore be used e.g. in atmospheric dispersion simulations. The advantage of using our algorithm with Sentinel-3A data lies in the previously demonstrated ability to detect and quantify small flares and the foreseen long term data availability from the Copernicus program. Our data (GFlaringS3, flaring activity and the related black carbon emissions) are available on the Emissions of atmospheric Compounds and Compilation of Ancillary Data (ECCAD) web site (https://eccad3.sedoo.fr/#GFlaringS3, DOI 10.25326/19 (Caseiro and Kaiser, 2019)) for use in, e.g., atmospheric composition modelling studies.

1 Introduction

Industrial gas flaring (GF) occurs when flammable gas is disposed of by burning, most commonly done at the tip of a stack. This can either take place as a measure for pressure relief, or to dispose of unwanted gas. In the upstream oil and gas (UOG) industry in particular, GF occurs when the associated gas can't be sold easily and is not used on-site for energy generation.

Especially in insufficiently developed energy markets companies seem to be spared from enough economic or political incentives to collect, or convert the gas. (Rahimpour and Jokar, 2012; Emeka Ojijiagwo et al., 2016) Improvements of flare gas recovery systems has been recommended for more closely monitored facilities (Zolfaghari et al., 2017; Papailias and Mavroidis, 2018).

https://doi.org/10.5194/essd-2019-99
Preprint. Discussion started: 25 July 2019

Open Access Earth System Science Data Discussions

GF negatively impacts the immediate surrounding (Akinola, 2018), for example through noise (Ismail and Umukoro, 2012; Nwoye et al., 2014), heat stress (Anomohanran, 2012; Julius, 2011) and visual pollution (Anomohanran, 2012; Ajao and Anurigwo, 2002). GF also impacts the environment on a wider scale through the emission of pollutants and greenhouse gases like carbon dioxide, carbon monoxide, black carbon, nitrogen oxides, polycyclic aromatic hydrocarbons, volatile organic compounds and acid rain precursors (Obioh et al., 1994; Uzomah and Sangodoyin, 2000; Nwaichi and Uzazobona, 2011; Onu et al., 2014; Li et al., 2016).

It has been estimated that between 2003 and 2012 GF produced on average 304 Tg CO_2 yearly, representing 0.6 % of the global anthropogenic emission of CO_2 equivalent (Olivier et al., 2014). The recovery of flare gas can play a relevant role in improving sustainability and meeting emissions targets. (Ahmed Osama Abdulrahman et al., 2015; Gabriele Comodi et al., 2016) Elvidge et al. (2018) estimated that a suppression of GF could contribute to 2% of the global nationally determined contributions (NDC) under the United Nations Framework Convention on Climate Change Paris Agreement. Some countries could meet or even surpass their NDC (Yemen, Algeria and Iraq), while others could meet between one third to almost all of their NDC (Gabon, Venezuela, Iran and Sudan).

Of particular importance is also the black carbon (BC) emission emitted by GF. BC is a known carcinogen (Heinrich et al., 1994) as well as a short-lived climate forcer (IPCC, 2013). BC strongly effects environments such as the Arctic regions through lowering the albedo of snow-covered surfaces (Flanner et al., 2007; Stohl et al., 2013; Bond et al., 2013; Huang et al., 2015; Evangeliou et al., 2018), impacting on the earth's radiative balance (Doherty et al., 2010; Quinn et al., 2007; Hansen and Nazarenko, 2004) as well as adding to the Arctic amplification phenomenon (Serreze and Barry, 2011). GF contribution to the BC global emissions was estimated to amount to 270 and 210 Gg in 2005 and 2010, respectively (Klimont et al., 2017). Regionally, Stohl et al. (2013) showed that GF contributes to half the near-surface BC concentration in the Arctic.

GF is considered an important component of atmospheric dispersion simulations (Evangeliou et al., 2018) and climate modeling (Huang and Fu, 2016) as the impact of GF emissions extends beyond immediate environmental concerns. However, information on the amount of natural gas being disposed of through stack burning and the accrued emissions are sparse. Reporting is often not enforced, inconsistent or otherwise not reliable.

Satellite remote sensing has been utilized for regional and global identification and characterization of GF. (Casadio et al., 2012b, a; Anejionu et al., 2014; Faruolo et al., 2014; Chowdhury et al., 2014; Anejionu et al., 2015; Faruolo et al., 2018) The most prominent system is NOAA's VIIRS (National Ocean and Atmospheric Administration's Visible Infrared Imaging Radiometer Suite) Nightfire dataset (see https://ngdc.noaa.gov/eog/viirs/download_viirs_fire.html), developed by Elvidge et al. (2016) based on previous work (Elvidge et al., 2001, 2007, 2009, 2013) and leading to a globally consistent survey of GF volumes available extending back to 2012.

We recently published an adaptation and extension of the VIIRS Nightfire algorithm with which observations of the Sea and Land Surface Temperature Radiometer instrument (SLSTR) on-board the Sentinel-3 satellites can be analysed, too (Caseiro et al., 2018). The algorithm detects and quantifies hot sources, including gas flares, using the night-time readings of the short-wave infrared (SWIR), mid-infrared (MIR) and thermal infrared (TIR) channels. The main advantages of using our hot spot detection and characterisation algorithm lie in the ability to detect and quantify smaller flares and the foreseen long term data

https://doi.org/10.5194/essd-2019-99
Preprint. Discussion started: 25 July 2019

availability from the series of Sentinel-3 satellites in the Copernicus program. Additionally, SLSTR observations (night-time overpasses at 10:00 PM) complement those of VIIRS (1:30 AM) by filling observation gaps in the time series.

Here, we describe a new dataset of global GF volume (Billion Cubic Meters, BCM) and BC emissions, which we have derived from all Sentinel-3 SLSTR observations in 2017. Chapter 2 describes newly developed methods for identifying gas flares among the observed hot sources, correcting for intermittent observations opportunities, and dynamically determining appropriate BC emission factors from the observations. The results of applying the hot source detection and characteristion algorithm plus the newly developed methods to all SLSTR observations of 2017 are presented in Chapter 3. Finally, our conclusions are summarised in Chapter 4.

2 Methods

2.1 Hot spot detection and characterization

An overview of the steps involved in the study presented here are outlined in Figure 1.

We base our work on the persistent hot spots detection and characterisation algorithm described in Caseiro et al. (2018) to process a full year (2017) of Sentinel-3A's Sea and Land Surface Temperature Radiometer (SLSTR) data. Using radiometrically calibrated radiance data as input, our algorithm detects hot spots and fits the sum of two Planck curves: one representing the hot source and the other the cool background. Both curves are fitted to the night-time spectral infrared (short-wave, mid-wave and thermal infrared: SWIR, MIR and TIR) observations to characterize temperature and area of the observed gas flares. Additionally, we calculate the radiative power of the flare using the Stefan-Boltzmann equation.

While in principle the methodology used is based on the Nightfire algorithm developed for Visible Infrared Imaging Radiometer Suite (VIIRS) (Elvidge et al., 2013, 2016), it differs by (1) analysing the radiances of clusters of contiguous hot pixels instead of treating spatial maxima as individual pixels and (2) using the TIR channels when fitting the sum of the two Planck curves. We expect the resulting gas flare representation to be more realistic and accurate for the characterisation of large gas flare arrays as well as for smaller flares and a more stringent constraining of the background temperature.

We already tested the method using oil and/or gas producing regions within a limited timespan and compared the results to the VIIRS Nightfire "flares only" product (Caseiro et al., 2018). The results showed a good agreement of our hot source detection when investigating persistent hot spots with the advantage of the Sentinel-3A's SLSTR algorithm in detecting and quantifying smaller flares, due to the night-time availability of a second SWIR channel. The characterisation (temperature, area and radiative power) also reached similarity although temperatures were slightly lower, whereas areas and radiative power were slightly larger in our results.

https://doi.org/10.5194/essd-2019-99
Preprint. Discussion started: 25 July 2019

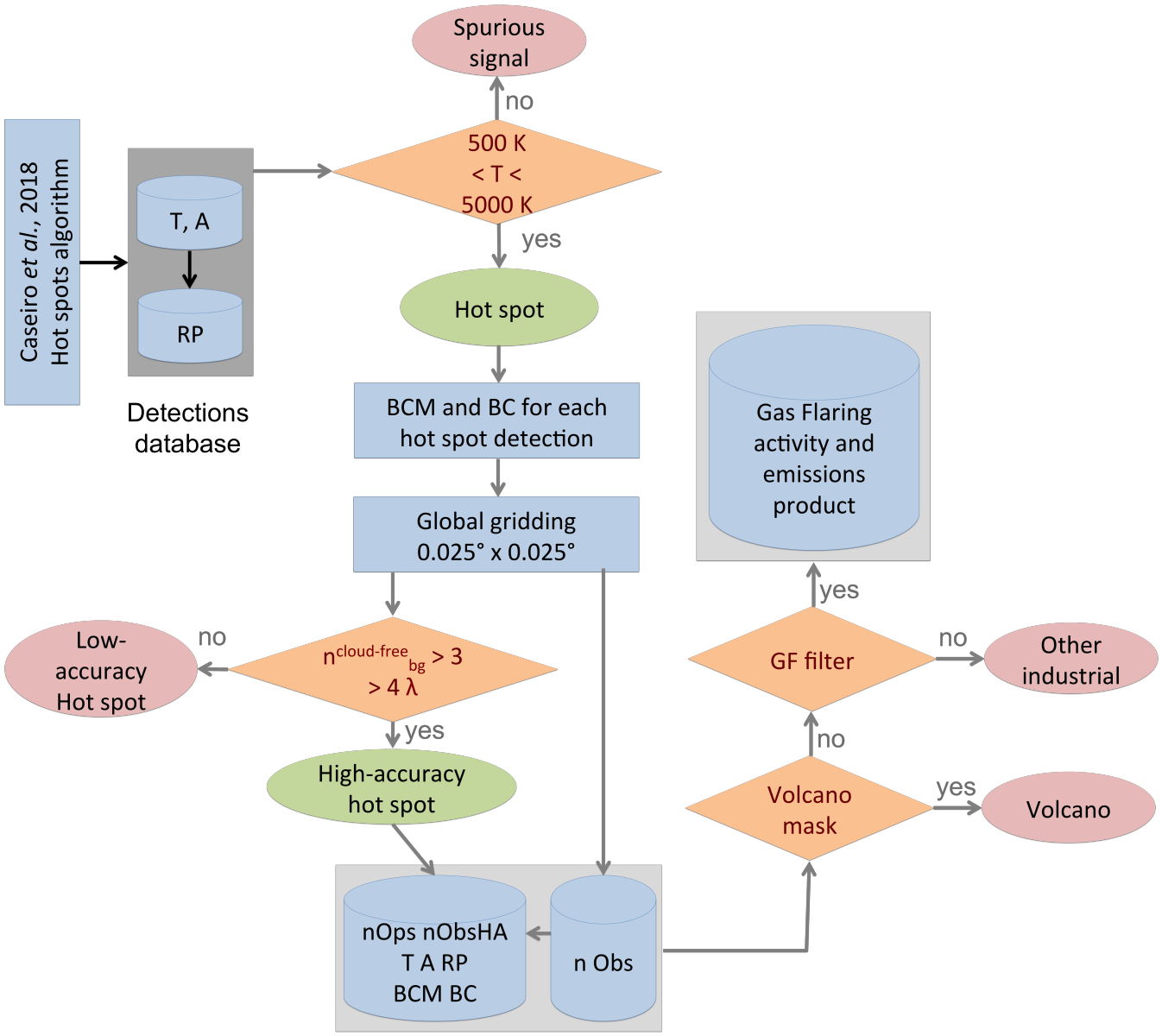

Figure 1. Flowchart of the methodology used in the present work. Starting point is the hot spot algorithm detection decribed in Caseiro et al. (2018) which, after applying a filter on the retrieved temperature (500 K $<$ T $<$ 5000 K), produces a database of hot spots detections. For each of these hot spot detections, the activity (Billion Cubic Meters, BCM) and Black Carbon (BC) emissions are computed. All hot spot detections are gridded into a global 0.025° $\times$ 0.025° grid. For each grid cell, the following quantities are computed: the number of detections, of high-accuracy detections and of days of detecion (see below, Section 2.2.2), temperature, area and radiative power (minimum, average, maximum and standard deviation), the date of the first and the last detection and the sum of the activity (BCM) and BC emissions. A volcano filter is applied to the global grid in order to mask out volcanic activity (see Section 2.2.1). The last step is the discrimination of grid cells for flaring activity (see Section 2.2.2).

https://doi.org/10.5194/essd-2019-99
Preprint. Discussion started: 25 July 2019

Open Access Earth System Science Data Discussions

2.2 Hot spot classification

2.2.1 Volcano filter

In order to filter out volcanic activity from our dataset, we use the data available from the Global Volcanic Program of the Smithsonian institution. (Venzke, 2013) The data was filtered for any eruption in 2017 and we computed a mask at the 0.025 degrees resolution. A buffering zone of 0.25° was used because the center coordinates specified may not correspond to the center of volcanic activity. Many volcanoes do not consist of a single edifice, but a volcanic field with many individual eruptive fissures through which lava erupts. (Siebert et al., 2010)

2.2.2 Discrimination of gas flares from other industrial hot sources

In order to discriminate gas flares from other night-time hot spots we investigate persistence and retrieval temperature filtering. We project all the hot spot detections onto a 0.025×0.025 degrees global grid. This is a spatial resolution which reflects the reality on the ground, where several flares, separated by tens to hundreds of meters, may be operated within a single oil and gas facility, while facilities are tens of kilometers apart. The following quantities are then computed for each grid cell: the number of hot spot detections (n_{Obs}), the number of high-accuracy (Caseiro et al., 2018) hot spot detections (n_{ObsHA}), the minimum, maximum, average and standard deviation of the high-accuracy hot spot retrieved temperature (T), area (A) and radiative power (RP) as well as the earliest and the latest hot spot observation date.

The temperature filtering we test is based on Elvidge et al. (2016) and on the recent work by Liu et al. (2018), who derived gas flaring temperatures of 1000 K to 2600 K from the VIIRS Nightfire database, depending on the type of operation (shale oil or gas, offshore, onshore or refinery). Most of the gas flares display temperatures between 1650 K and 1850 K. However, temperatures can occasionally be as low as 1300 K. This overlaps with particularly hot detections from the coal chemical industry and steel plants. Therefore, additional criteria are needed for identifying gas flares in the hot source dataset.

In order to select the discriminating strategy we test several subsets of the hot spot database. For each subset described in Table 1, a sample of 100 random onshore grid cells have been tested by examining high-resolution imagery (Google Earth) and the locations are classified into four categories:

Flare (F) flaring site with visible flame

Likely (L) industrial or oil extraction site with typical flaring infrastructure but no visible flame

Unlikely (U) industrial site without typical flaring infrastructure

No industry (N) e.g. agricultural or forested area.

The subsets are characterized in terms of user's accuracy (Equation 1) and commission error (Equation 2).

$$User's\ accuracy = \left(F + \frac{L}{2}\right) \pm \frac{L}{2} \tag{1}$$

https://doi.org/10.5194/essd-2019-99
Preprint. Discussion started: 25 July 2019

Open Access Earth System Science Data Discussions

Table 1. User's accuracy (UA, %) and commission error (C, %) of the hot spot discrimination strategies considered.

n_{Obs} >	–	3	4	–	–	–	–	–
n_{ObsHA} >	2	2	2	5	5	5	7	7
T_{min} (K) >	1000	1000	–	–	–	–	–	–
T_{max} (K) >	1400	1400	800	1200	1500	1800	1200	1500
n_{cells}	6733	5872	9469	6817	6232	5485	5527	5129
UA	84±6	86±8	60±10	77±13	85±11	88±10	73±14	87±11
C	7±3	4±2	19±11	6±4	3±1	1±1	8±5	2±1

$$Commission\ error = \left(N + \frac{U}{2}\right) \pm \frac{U}{2} \tag{2}$$

In some industrial areas, facilities that use gas flares may be close to other hot spots, such as iron smelters or steel mills. In those cases, a commission error occurs when the flare is off and our methodology samples the other hot spot. The omission error can be divided into two categories: flares that the hot spot detection and characterization algorithm failed to detect and flares that were detected as hot spots but which the discrimination strategy left out. The former will be the same for any discrimination procedure considered.

Detections located in grid cells where the yearly maximum temperature retrieval is above 1500 K and a persistency and quality criterion ($n_{ObsHA} > 5$) is met are considered as originating from gas flares and called flaring locations hereafter. This achieves a relatively large number of grid cells with detections, i.e. low omission error, combined with a high user's accuracy and a low commission error of 85±11% and 3±1%, respectively. Inserting a limitation on the minimum temperature or increasing the maximum temperature or the number of high-accuracy observations would not significantly increase the user's accuracy or decrease the commission error, but would reduce the number of grid cells complying to the discrimination criteria by several hundreds, which we interpret as an increase in the omission error.

2.3 Determination of flared volumes and black carbon emissions

In order to compute the activity and emissions, we estimated the number of days of operations per site by expressing the maximum number of observations as a function of latitude (in 10° bins, see Figure 2). The function computes the maximum number of observations ($nObs_{max}$) per grid cell for a given latitude which we assume expresses a continuous hot spot (365 days a year). The number of days of operation is then estimated by scaling following Equation 3. By this scaling, we take into consideration the limitations of gas flaring detection from space (cloud cover and overpass frequency).

$$n_{Ops} = n_{Obs} \times \frac{365}{n_{Obs_{max}}} \tag{3}$$

https://doi.org/10.5194/essd-2019-99
Preprint. Discussion started: 25 July 2019

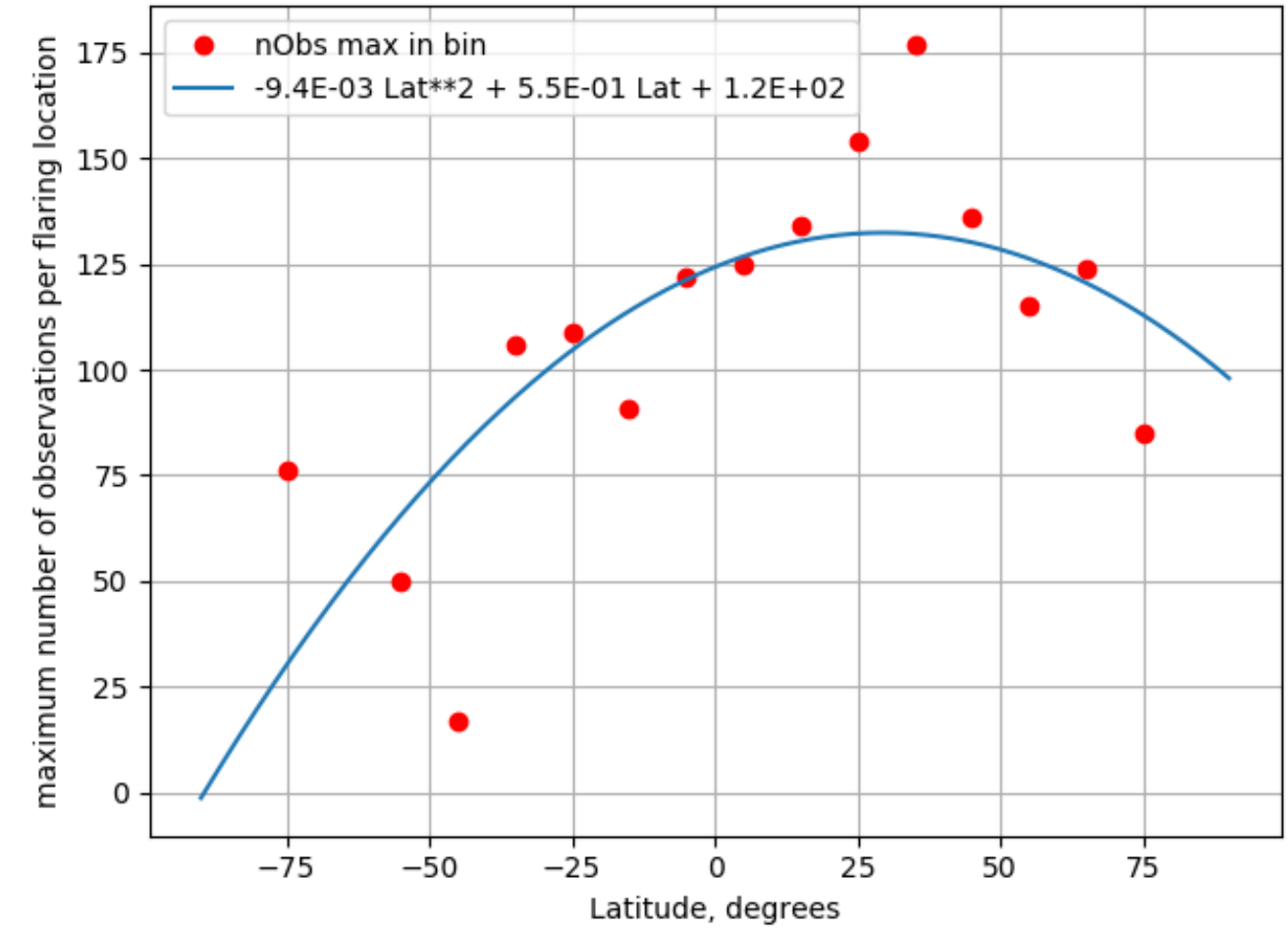

Figure 2. Maximum number of observations per grid cell as a function of Latitude. The latitude values are binned (10°). The function expresses the maximum number of observations $n_{Obs_{max}}$, which we assume as a continuous operation of the hot source, as a function of latitude.

https://doi.org/10.5194/essd-2019-99
Preprint. Discussion started: 25 July 2019

Open Access Earth System Science Data Discussions

For the estimation of the flared volume, we applied the calibration derived by Elvidge et al. (2016) to each single detection within a flaring location grid cell. The calibration relationship uses a modified formulation of the radiative power to output the yearly flared volumes (in Billion Cubic Meters, BCM), which is then scaled to a daily activity in m^3.

The best activity estimate corresponds to assuming that the flare is active for n_{Ops} days:

$$BCM_{best} = BCM_{min} \times \frac{n_{Ops}}{n_{Obs}} \tag{4}$$

The lower bound BCM_{min} for the activity estimate assumes that the flare is only active on the n_{Obs} days with hot spot detections. The upper bound for the activity estimate assumes that the flare is constantly active:

$$BCM_{max} = BCM_{min} \times \frac{365}{n_{Obs}} \tag{5}$$

The emissions of black carbon (BC) from gas flares are estimated using reported emissions factors (EF). Stohl et al. (2013) used an EF of 1.6 $g.m^{-3}$, while Schwarz et al. (2015) and Weyant et al. (2016) conducted field experiments in the Bakken formation (USA) and derived EFs of 0.57±0.14 $g.m^{-3}$ and 0.13±0.36 $g.m^{-3}$ (using the Single Particle Soot Photometer) or 0.28 $g.m^{-3}$ (using the Particle Soot Absorption Photometer), respectively. However, flared gas has not the same composition everywhere and Huang and Fu (2016) considered the regional variability of the EF. The authors applied the function which relates EF to the volumetric gas heating value derived in the laboratory by McEwen and Johnson (2012) to globally compiled gas composition data. Klimont et al. (2017) considered, for the Greenhouse Gas – Air Pollution Interactions and Synergies (GAINS) model, the EF derived by Schwarz et al. (2015) of 0.57 $g.m^{-3}$ for well-operated flares (i.e. Organisation for Economic Co-operation and Development (OECD) countries) and a maximum of 1.75 $g.m^{-3}$ for other countries. In the present work, we apply the same concept of a varying EF but use the flare temperature as an indication of the combustion completeness, instead of the country of origin as an indication of the flare operation. Flaring temperatures close to the adiabatic flame temperature for natural gas (around 2500 K) are associated with more complete combustion and therefore lower BC emissions. On the other hand, low flaring temperatures (700 K and below) are associated with higher BC emissions. Between the two extremes, the BC emission is scaled linearly as a function of the flaring temperature (see Figure 3). To the best of our knowledge, this is the first time that operating practices are taken into consideration when assigning the EF.

The country-level BCM and BC estimates are computed by summing the individual flares estimates within the borders of each country and its exclusive economic zone.

With this methodology we estimate a wide range of possible activity (BCM) and emissions (BC), where our best estimate falls between the 'flaring only when there is a detection' (BCM_{min} and BC_{min}) and 'always flaring' (BCM_{max} and BC_{max}). We conservatively assume that this range of possibilities represents $6 \times \sigma$, and report the uncertainty of the best estimates as $1 \times \sigma$.

https://doi.org/10.5194/essd-2019-99
Preprint. Discussion started: 25 July 2019

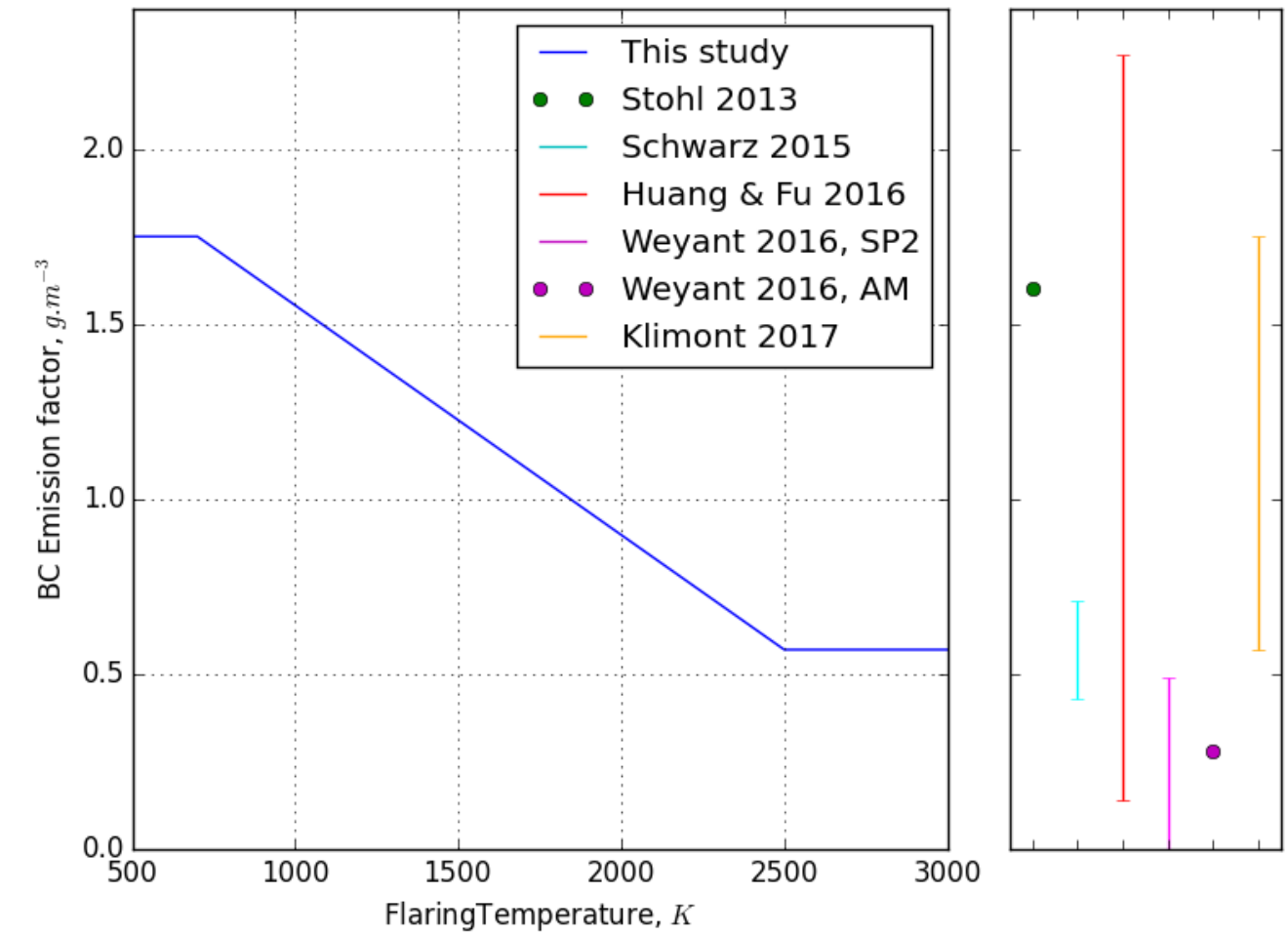

Figure 3. Left: BC emission factor function used in the present study. The emission factor is bounded by the extremes of the range used in the GAINS model (Klimont et al., 2017) and scaled as a function of the flaring temperature, used as an indication of combustion completeness. Right: For comparison purposes, the EFs derived by Stohl et al. (2013); Schwarz et al. (2015); Huang and Fu (2016), Weyant et al. (2016) (using the Single Particle Soot Photometer, SP2, or the Particle Soot Absorption Photometer, AM) and Klimont et al. (2017).

https://doi.org/10.5194/essd-2019-99
Preprint. Discussion started: 25 July 2019

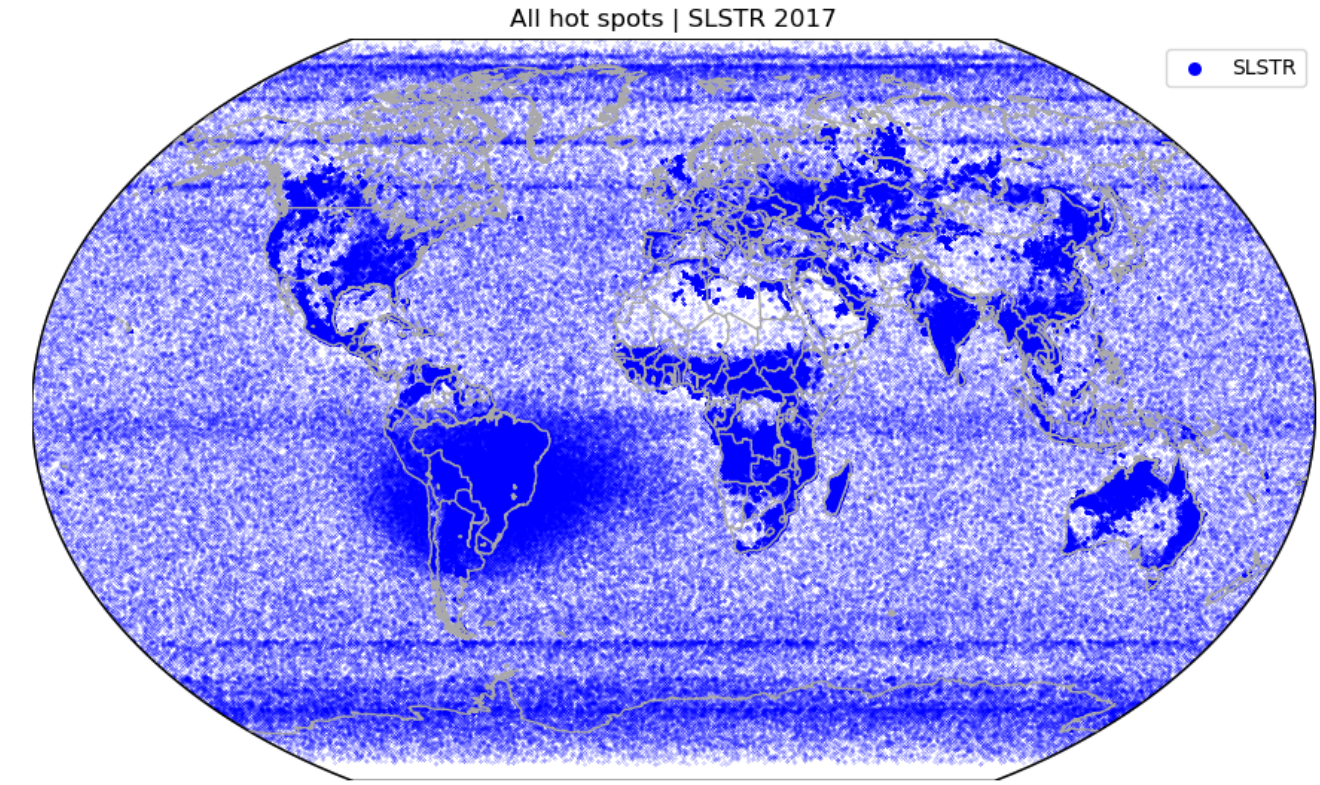

Figure 4. Location of all the 807327 hot spots (all detections database filtered for spurious signals, see Figure 1), detected in 2017.

3 Results

3.1 Hot spots and flaring sites

All the hot spots detected globally for 2017 using the algorithm as described in Figure 1 are shown in Figure 4. The data is available online at the ECCAD webpage (Caseiro and Kaiser, 2019). The algorithm detected 807327 hot spots.

Noise, such as detections in the open ocean and the South Atlantic anomaly, is filtered out when considering only the high-accuracy hot spots as defined by Caseiro et al. (2018). There are 95906 high-accuracy hot spots in the dataset. These are shown in Figure 5. Their distribution pattern suggests that they encompass a large range of hot sources, such as wildfires, volcanoes and industrial sources.

After gridding, filtering out active volcanoes (our methodology, see Section 2.2.1, accounted for 71 volcanic eruptions in 2017) and retaining the grid cells passing the GF criteria (see Section 2.2.2) the number of globally detected flaring sites in 2017 are 6232, see Figure 6. This is lower than the estimate of 7467 by Elvidge et al. (2016). Although our Sea and Land Surface Temperature Radiometer (SLSTR)-based methodology is able to detect smaller gas flares due to the availability of

https://doi.org/10.5194/essd-2019-99
Preprint. Discussion started: 25 July 2019

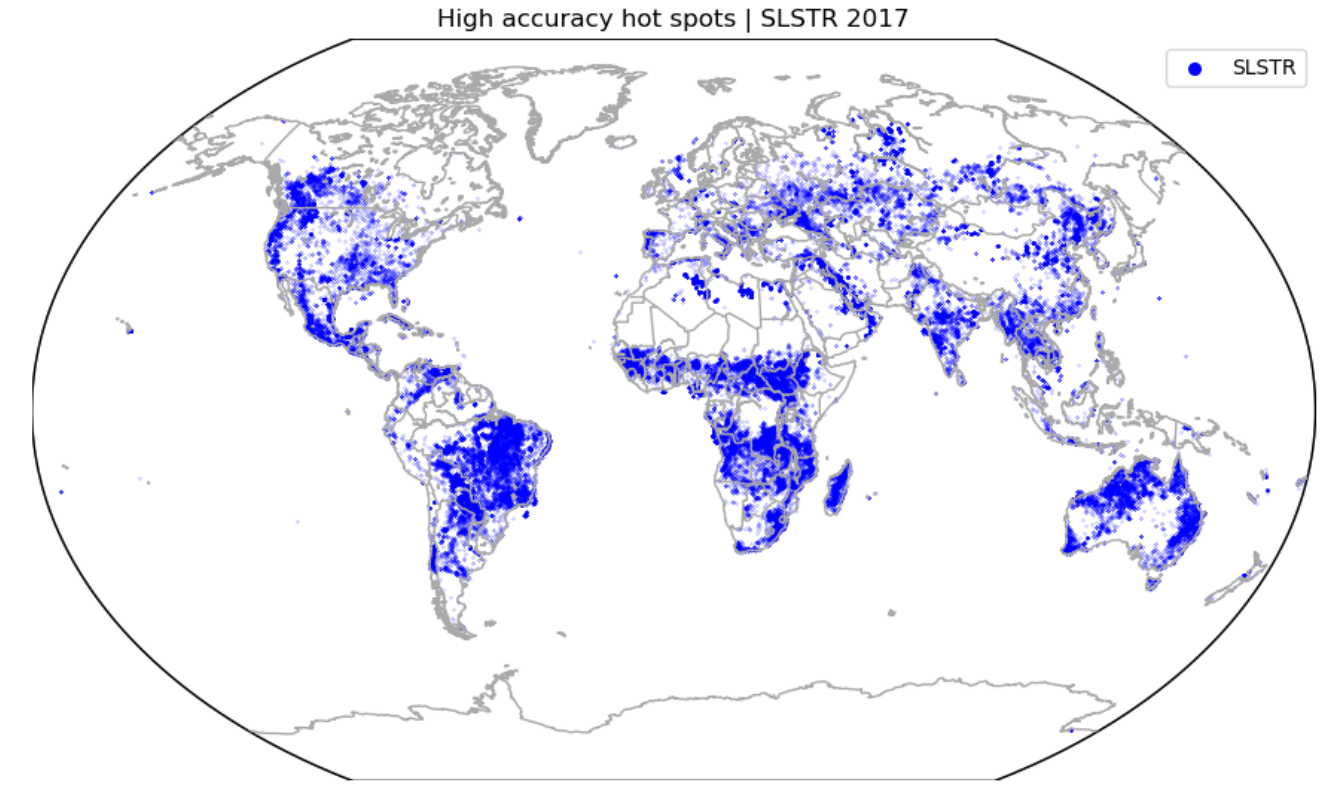

Figure 5. Location of all the 95906 high-accuracy hot spots (gridded hot spots filtered for cloudiness and accuracy of the Planck curve fitting, see Figure 1), detected in 2017.

the second SWIR channel, the Visible Infrared Imaging Radiometer Suite (VIIRS) Nightfire algorithm is expected to detect a larger number of hot spots because it considers local maxima, whereas our methodology clusters adjacent hot pixels.

Russia (985) and the United States (917) are the countries with the highest number of flaring locations. The third country is Iran (441) with less than half of the top two countries. The five countries with more than 300 flaring locations – China (365) and Algeria (324) in addition to the top 3 – account for about one half of the global flaring locations. The United States is the country with the largest difference in the number of flaring locations between 2017 (this work, 917) and 2012 (2399, as reported by Elvidge et al. (2016)). Besides the aforementioned methodological difference, a switch from well-product testing to formal operation could be the reason for a lower number of detected flaring sites (Liu et al., 2018). Such a transition from a higher number of lower intensity flares to a smaller number of higher intensity flares was reported between 2012–2014 and 2015–2016 by Franklin et al. (2019) for the Eagle Ford shale region of South Texas.

The time series of the cumulative number of the high accuracy observations for the most active flaring location (in Venezuela, see Section 3.4) is shown in Figure 8. It shows flaring activity throughout the year.

https://doi.org/10.5194/essd-2019-99
Preprint. Discussion started: 25 July 2019

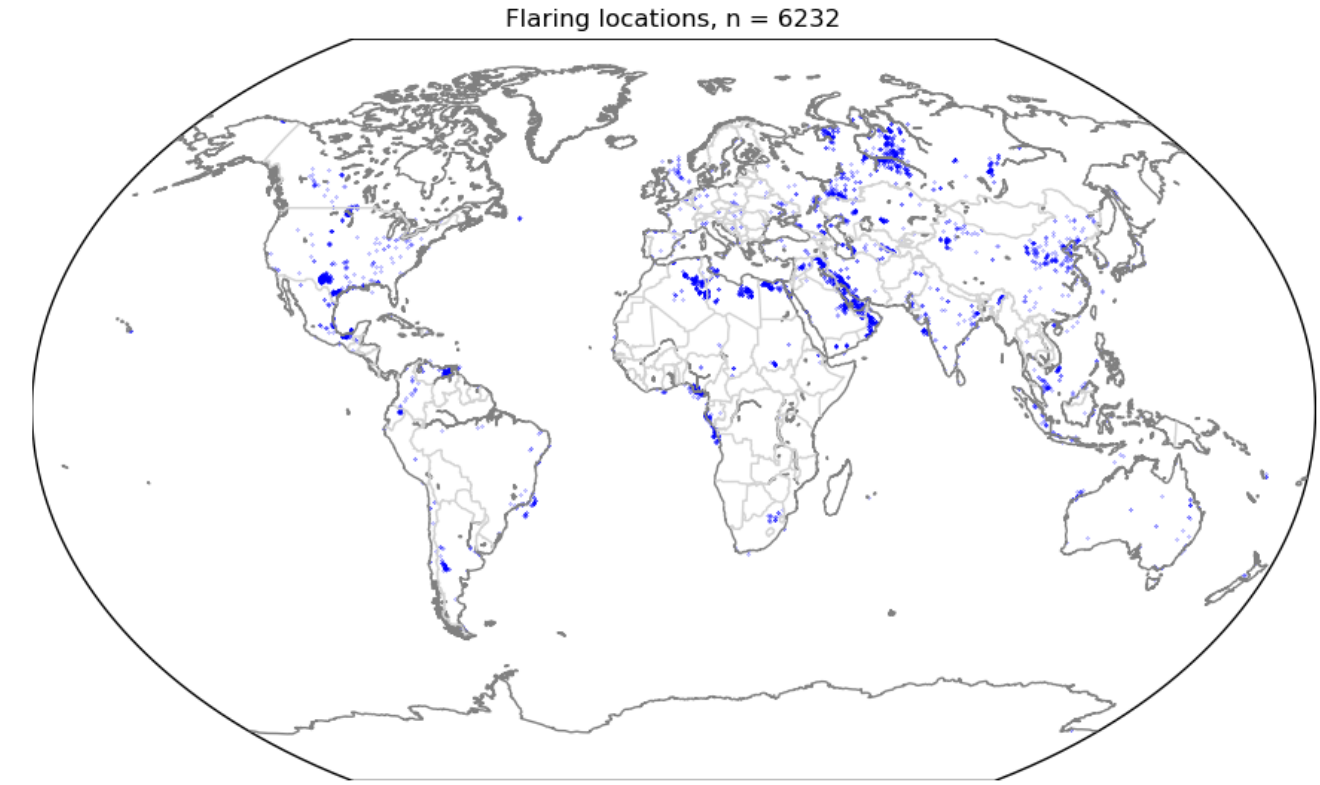

Figure 6. Location of all the 6232 flaring locations (grid cells with at least 5 high-accuracy hot spots and a maximum retrieved temperature above 1500 K) detected in 2017.

3.2 Flaring characteristics

Statistics on retrieved temperature and radiative power are reported in Figures 9 to 13.

The average temperature at the flaring locations approximately ranges from 950 K to 2250 K. This is slightly lower than the range reported by Liu et al. (2018) who used Visible Infrared Imaging Radiometer Suite (VIIRS) Nightfire data, as expected from our previous study (Caseiro et al., 2018). It confirms the bi-modal distribution with modes around 1750 K and 1200 K that is has also been observed by VIIRS.

One of the most active flaring regions of the world is the Persian gulf. Figure 10 shows the average retrieved temperature at flaring locations in that region, while the time series of the retrieved flaring temperatures is shown in Figure 11. The time series of the retrieved temperature for the most active flaring location (in Venezuela, see below, section 3.4) is shown in Figure 12.

The average radiative power at flaring locations range from a few tenths of MW up to approximately 1 GW (Figure 13), spanning the 5 orders of magnitude reported by Elvidge et al. (2016).

https://doi.org/10.5194/essd-2019-99
Preprint. Discussion started: 25 July 2019

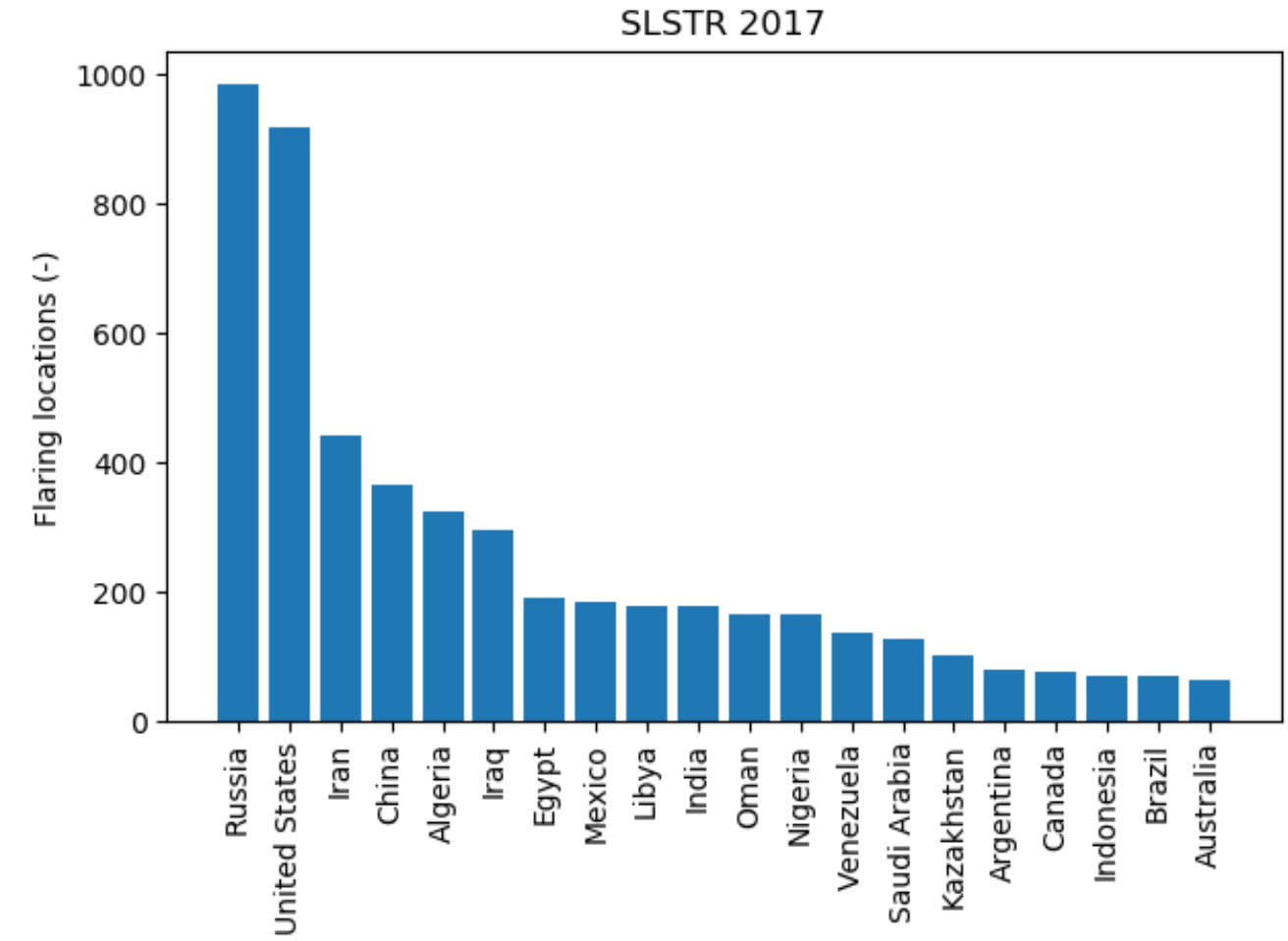

Figure 7. Flaring locations by country, top 20.

3.3 Comparison with VIIRS Nightfire

We compare our results to the data set from the Visible Infrared Imaging Radiometer Suite (VIIRS) Nightfire 2017 results made available by the National Geophysical Data Center of the National Oceanic and Atmospheric Administration of the United States at https://www.ngdc.noaa.gov/eog/viirs/download_viirs_fire.html. Figure 15 shows all Nightfire detections in 2017 (green), projected onto the same 0.25° × 0.25° global grid as for our results (see above, sections 2.2.2 and 3.1).

In order to segregate the flaring signal from other hot spots, we adapt the thresholds we used for hte Sea and Land Surface Temperature Radiometer (SLSTR). The persistency threshold was adjusted from 5 (for a 1400 km swath for SLSTR) to 11 detections a year within a grid cell (for a 3040 km swath for VIIRS). The lowest yearly maximum temperature retrieved within a grid cell was maintained at 1500 K. Grid cells which comply to these criteria are shown in Figure 15 (red). These adapted

https://doi.org/10.5194/essd-2019-99
Preprint. Discussion started: 25 July 2019

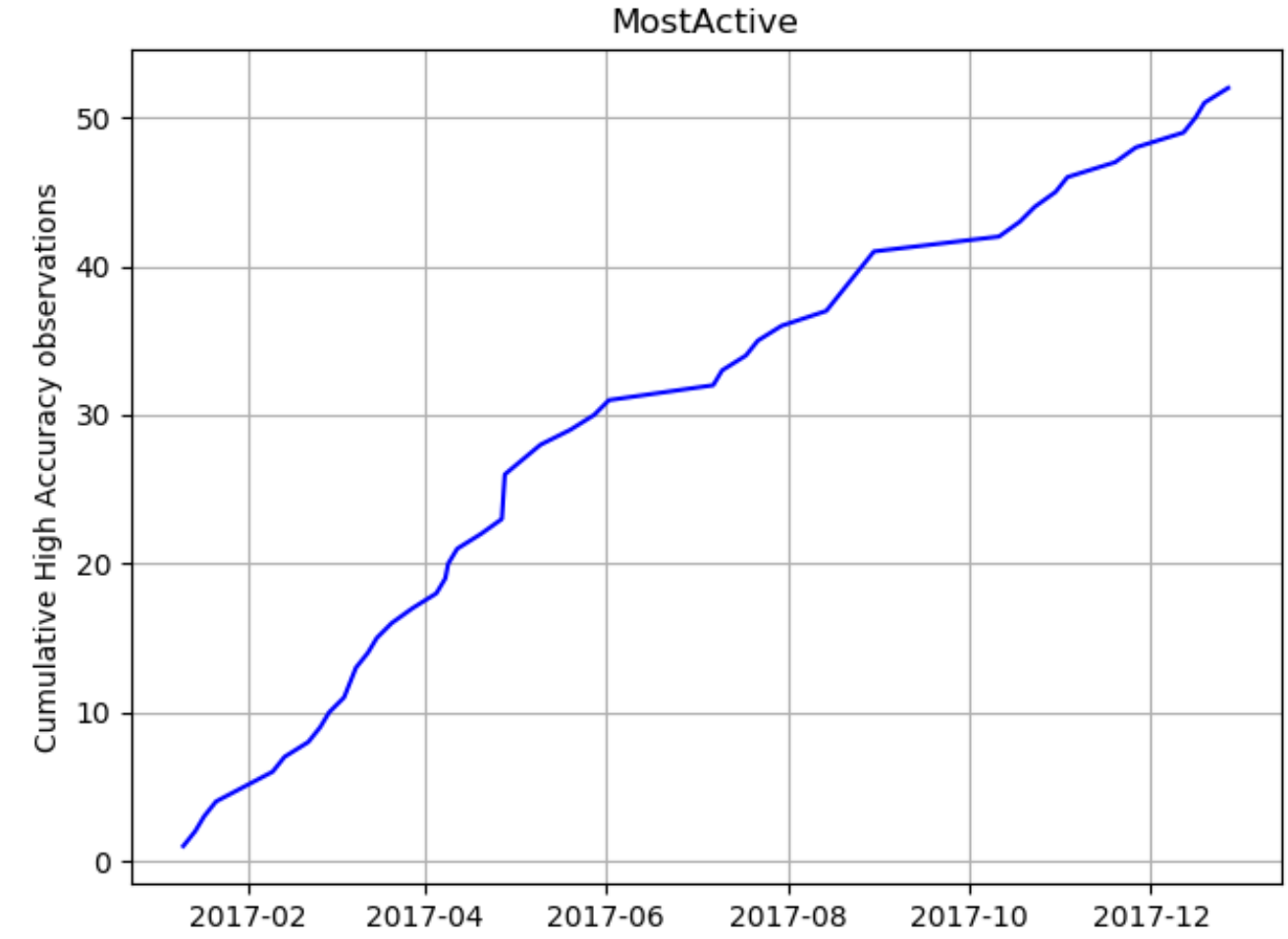

Figure 8. Cumulative number of high accuracy observations at the most active flaring location (52 high accuracy detections over 47 days at the grid cell centered at 63.6875°W, 9.6375°N).

https://doi.org/10.5194/essd-2019-99
Preprint. Discussion started: 25 July 2019

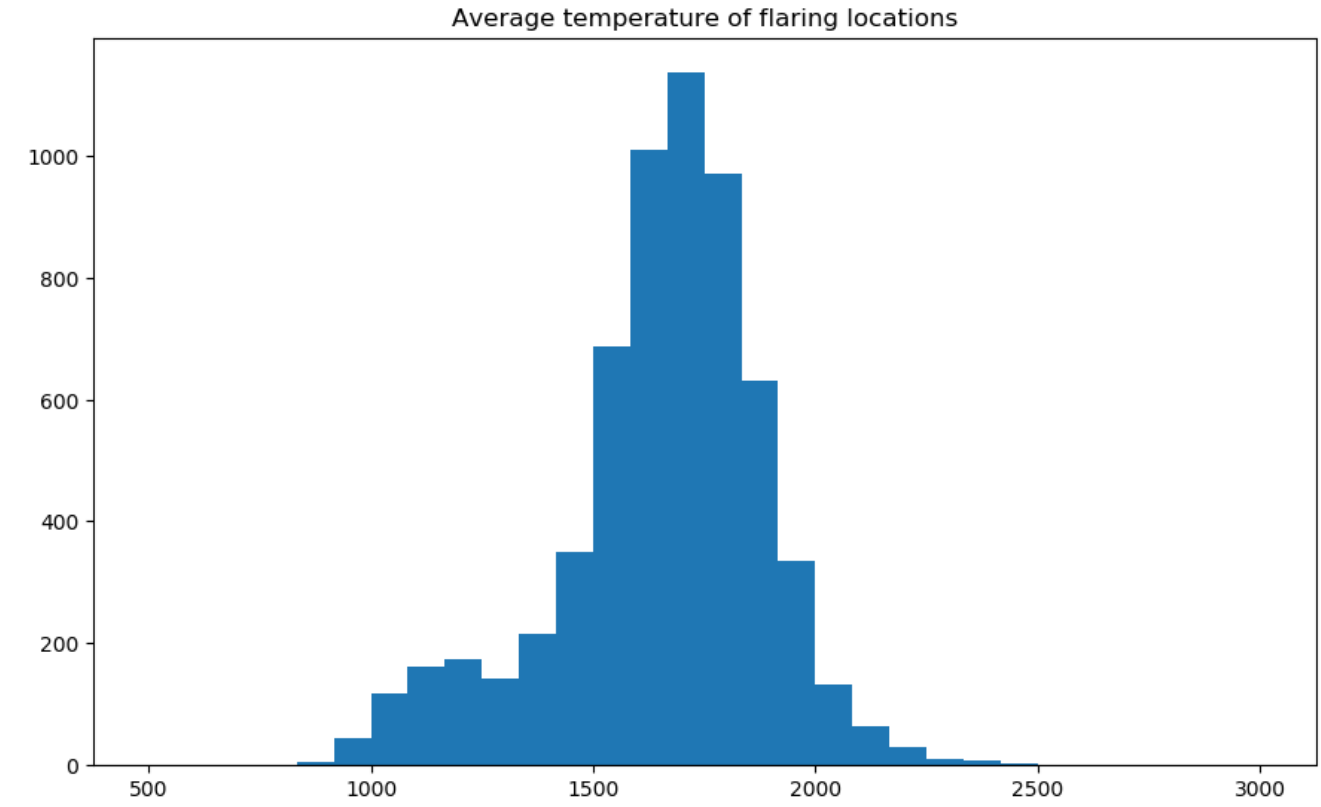

Figure 9. Distribution of the average retrieved hot spot temperature (K) for the flaring locations.

thresholds filter out a very large number of hot spots and produce a global VIIRS Nightfire flaring map similar to that obtained by our methodology based on SLSTR observations (see Figure 6). Despite this global agreement, some significant regional differences are visible: the Western U.S. and Canada, the Amazonian forest, Australia, Eastern and Western China. Liu et al. (2018) referred to this last region as "undetected oil/gas heat source" in Elvidge et al. (2016). The number of detected VIIRS Nightfire flaring locations (18855) is about three times that returned by our methodology (6232). Such a behaviour is expected because the Nightfire algorithm considers pixels which are local maxima and our methodology aggregates contiguous hot pixels within a same cluster. These clusters may be very large and contain more than one local maximum.

The distribution of the retrieved average flaring temperatures at each site is very similar, as shown in Figure 16.

3.4 Flared volumes

The activity for all the individual flaring locations is shown in Figure 17. The distribution is very close to that reported by Elvidge et al. (2016), with the exception of the very few extremes in the range 0.8–1.1. The most active flare burned 0.623 BCM throughout 2017 and is located south of Punta de Mata in Venezuela. This is also where Elvidge et al. (2016) found the

https://doi.org/10.5194/essd-2019-99
Preprint. Discussion started: 25 July 2019

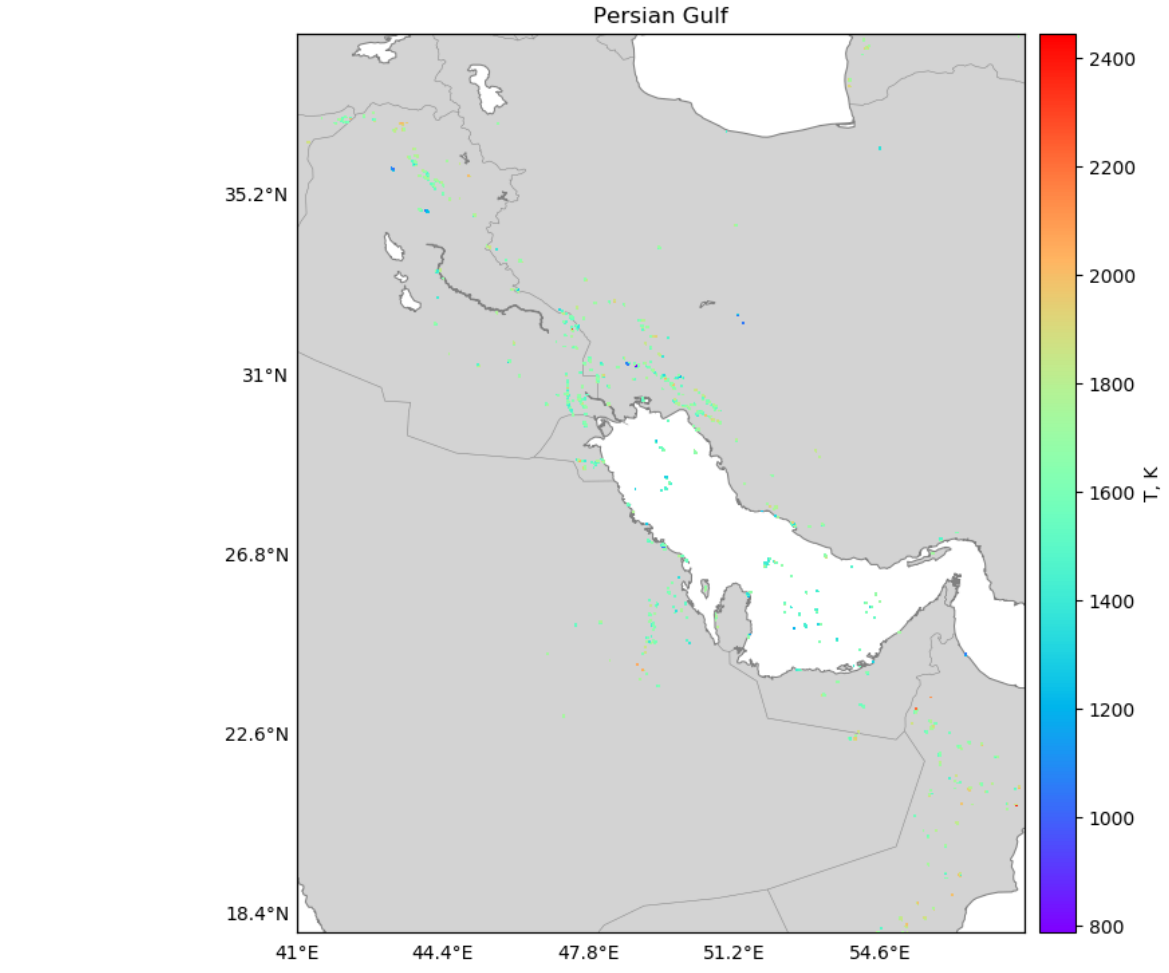

Figure 10. Average flaring temperature (K) at flaring locations in the region of the Persian gulf (1184 flaring locations in the region, aggregated from 41600 high-accuracy detections over 348 days).

https://doi.org/10.5194/essd-2019-99
Preprint. Discussion started: 25 July 2019

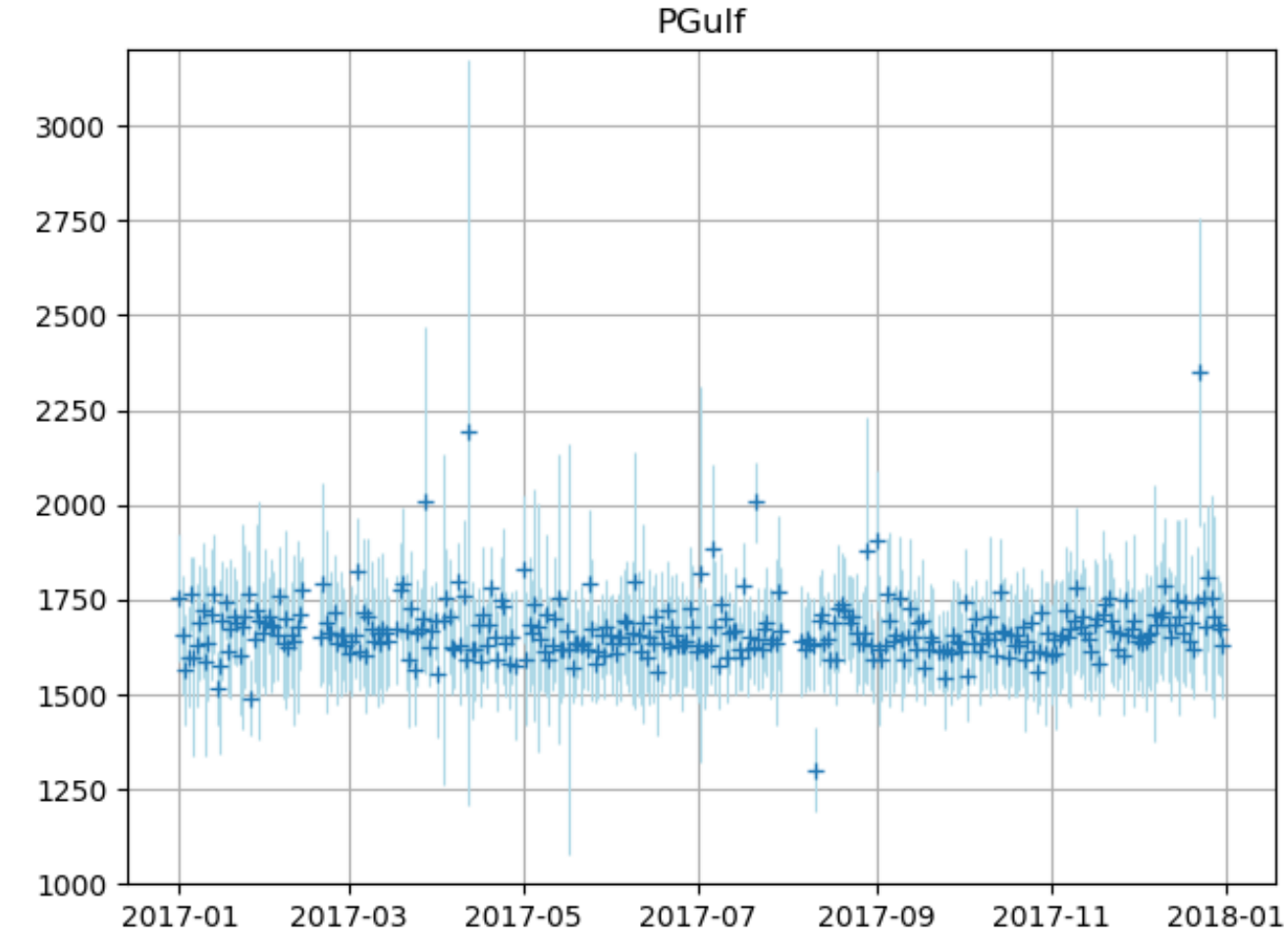

Figure 11. Time series of the daily average retrieved flaring temperatures (K, the bounds represent 1 standard deviation) in the region of the Persian gulf (41600 high accuracy detections over 348 days at 1184 flaring locations) shown in Figure 10.

https://doi.org/10.5194/essd-2019-99
Preprint. Discussion started: 25 July 2019

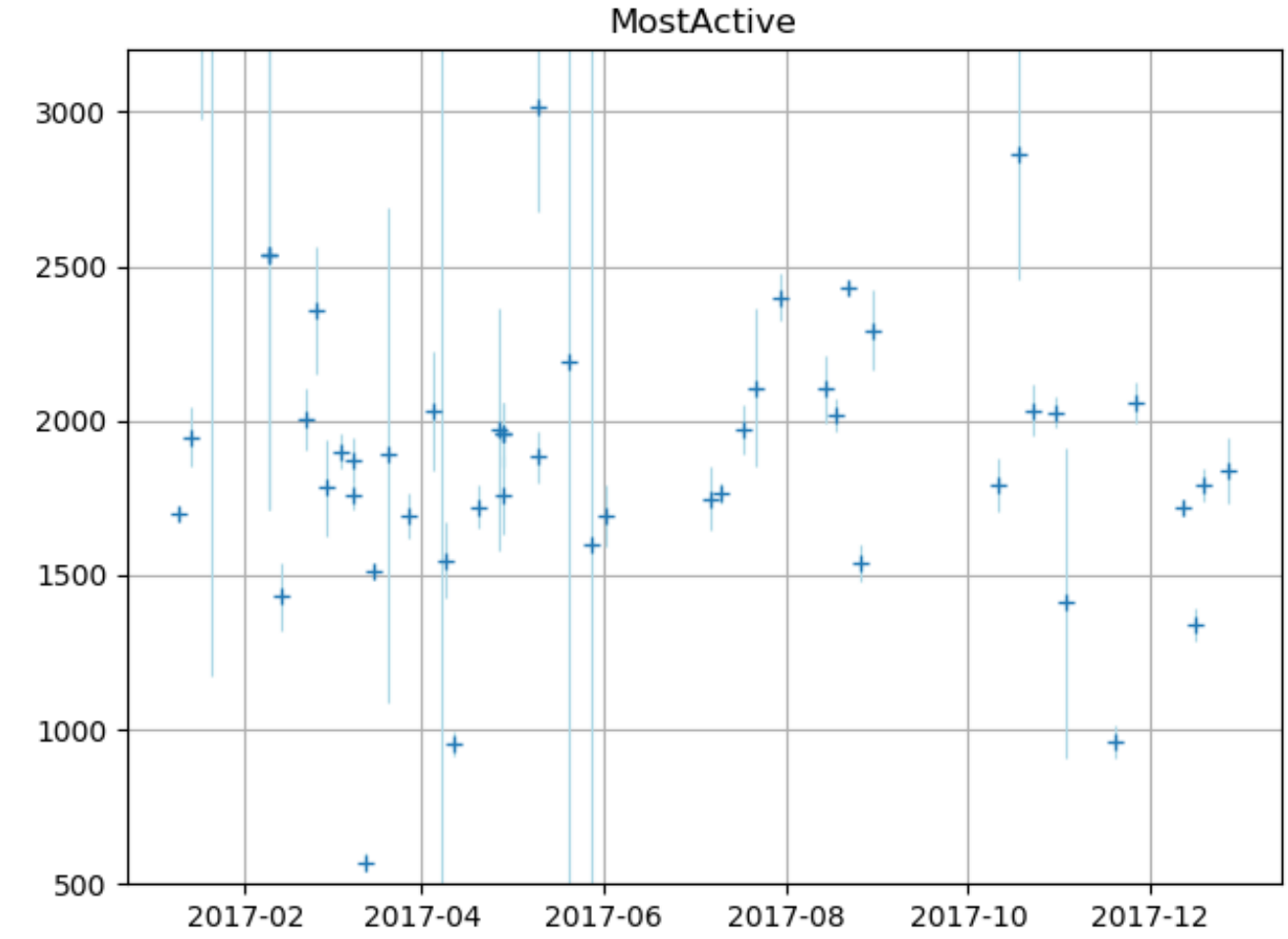

Figure 12. Time series of the retrieved temperatures (with bounds) at the most active flaring location (52 high accuracy detections over 47 days at the grid cell centered at 63.6875°W, 9.6375°N in Venezuela).

https://doi.org/10.5194/essd-2019-99
Preprint. Discussion started: 25 July 2019

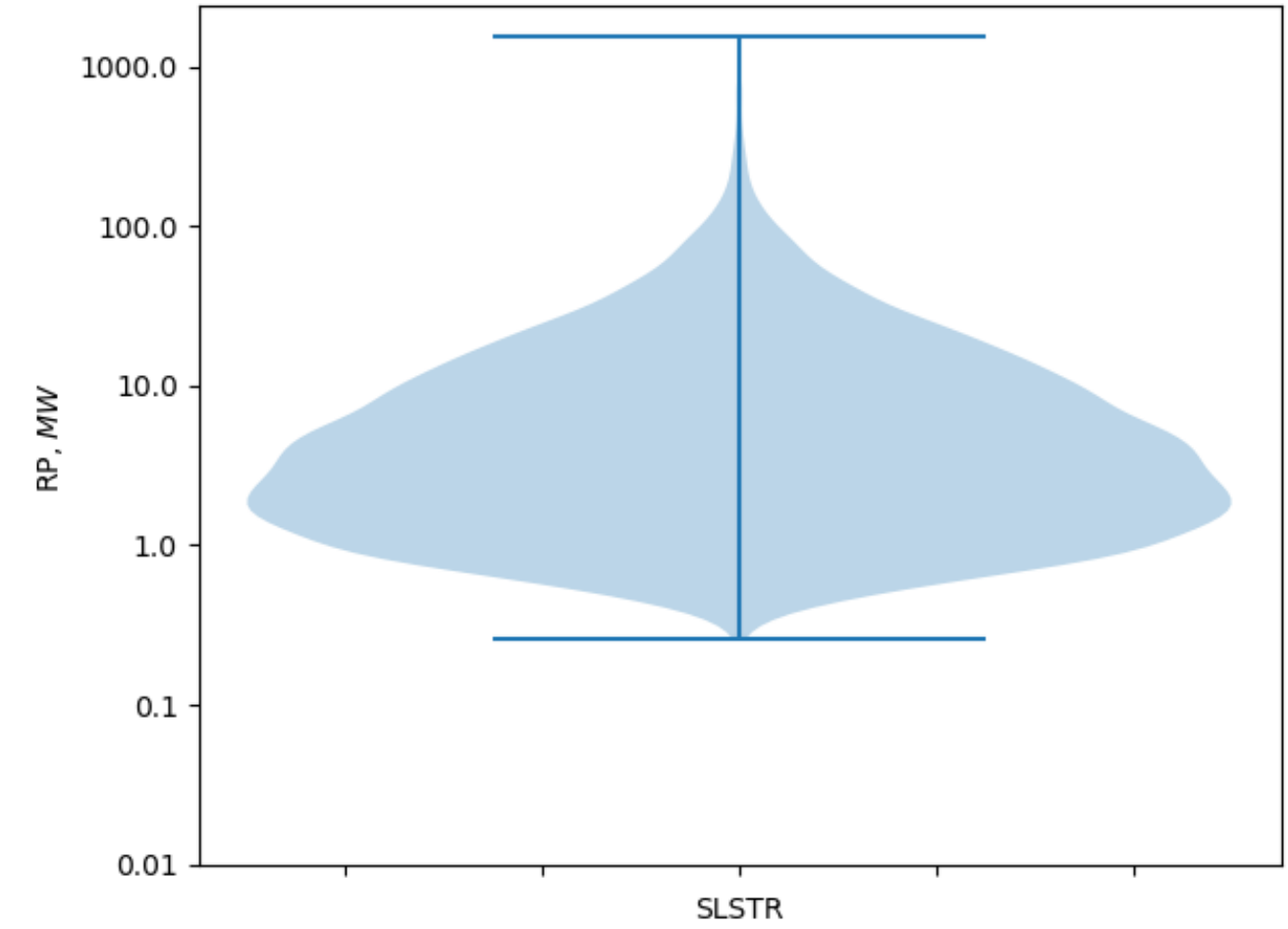

Figure 13. Distribution of the average radiative power (MW) for the 6232 global flaring locations.

most active flare for 2012, though more active (1.13 BCM). The total activity of the region is shown in Figure 18, and the cumulative activity throughout the year in Figure 19.

Our best estimate for the global flared volume for 2017 is 129±64 BCM. This is slightly lower than the 143±13.6 BCM reported by Elvidge et al. (2016) for 2012. The lower and upper bounds of the range of possibilities for the estimate are 35.0 BCM (there is flaring only when there is a detection) and 419.1 BCM (flaring is always on), respectively.

Approximately half of the global flared volume originates from 4 countries only: Iraq (19.0 BCM), Iran (18.4 BCM), Russia (18.1 BCM) and Algeria (10.5 BCM).

https://doi.org/10.5194/essd-2019-99
Preprint. Discussion started: 25 July 2019

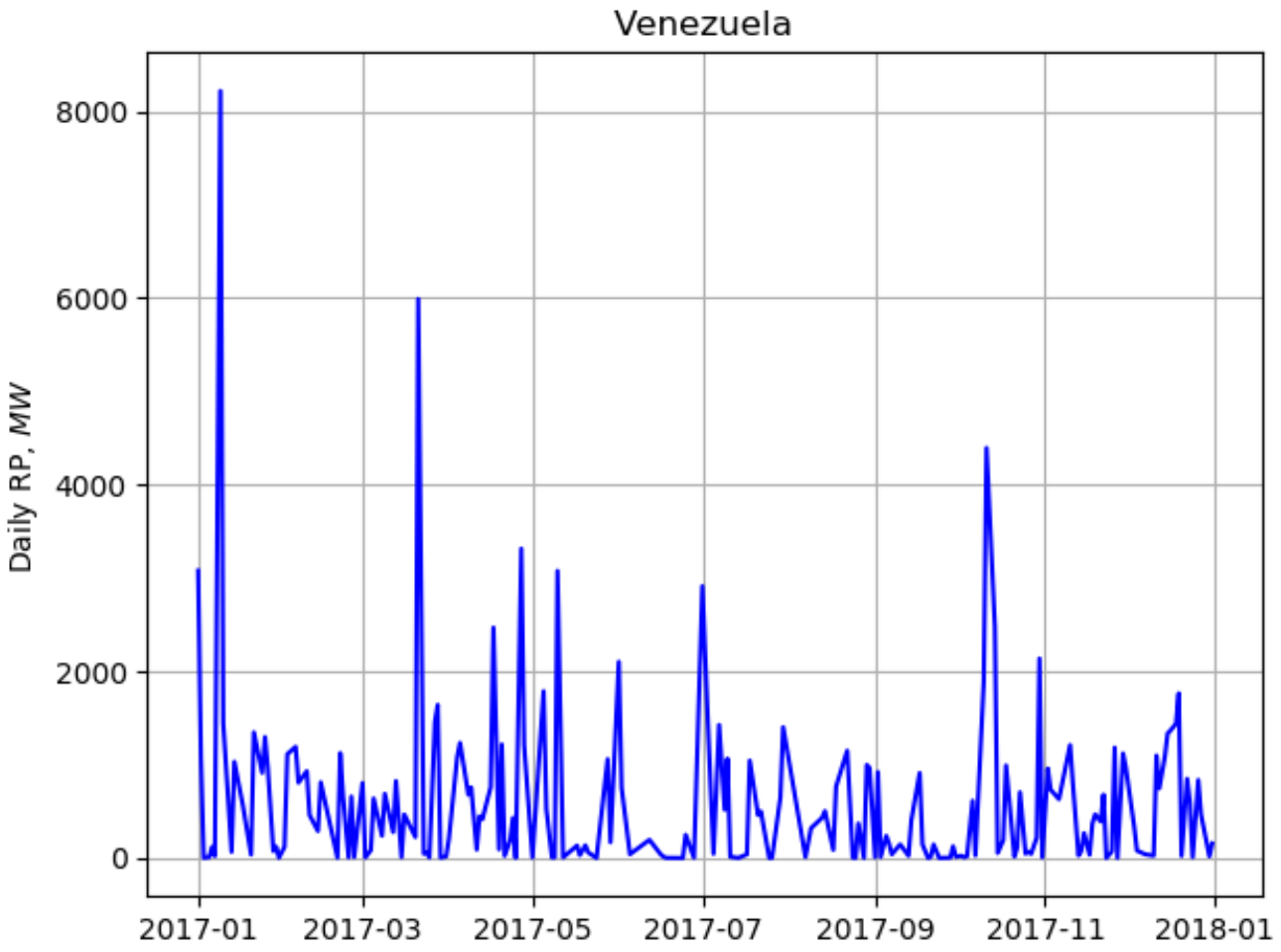

Figure 14. Time series of the total radiative power (MW) in the oil producing region of Venezuela (2391 high accuracy observations at 112 flaring locations over 200 days), where the most active flare is located (see below, section 3.4).

https://doi.org/10.5194/essd-2019-99
Preprint. Discussion started: 25 July 2019

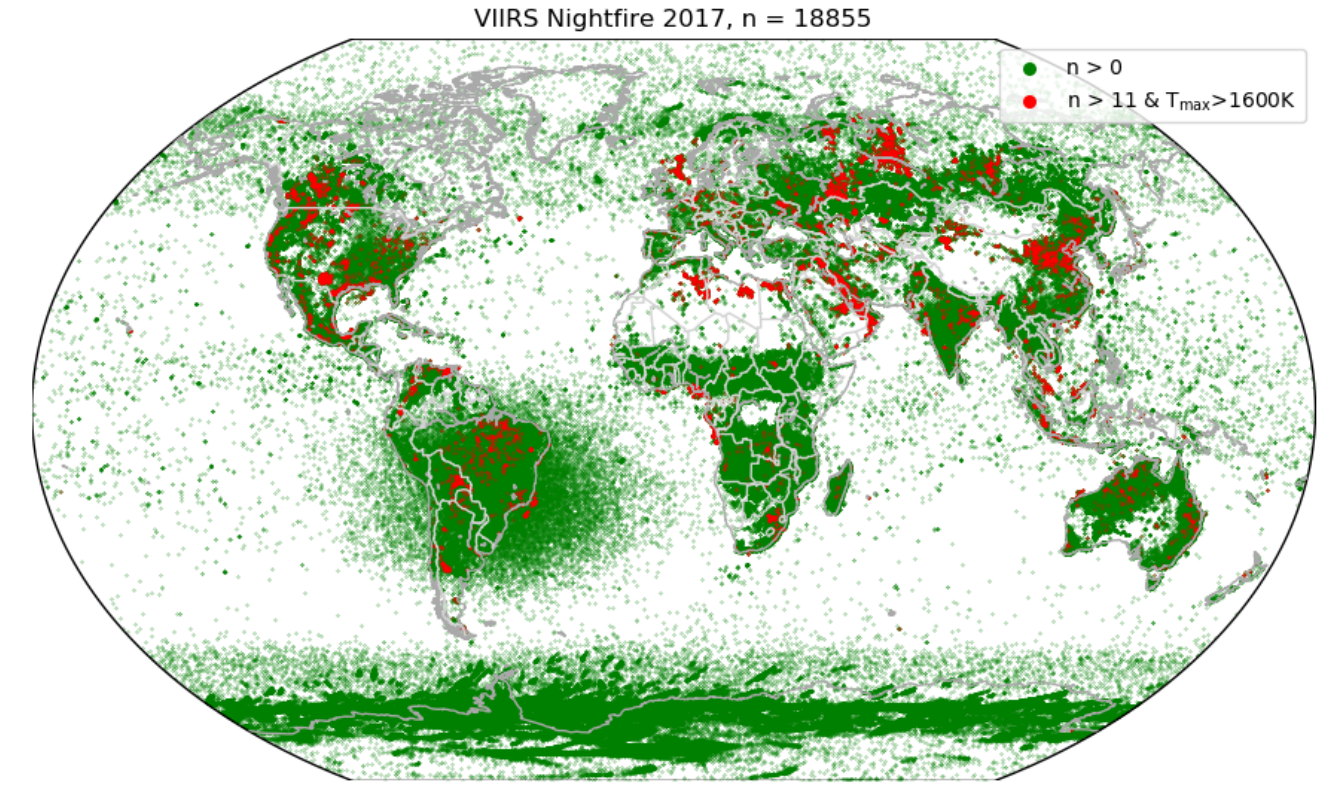

Figure 15. VIIRS Nightfire locations (all locations, green, and flaring locations, red) for 2017. The flaring locations were derived by adapting our SLSTR flaring location thresholds to the VIIRS sensor characteristics: at least 11 detections within the grid cell and at least 1600K as the maximum temperature detected within the grid cell.

3.5 BC emissions

The black carbon (BC) emissions for all the individual flaring locations are shown in Figure 21. The most active flare emitted 0.35 Gg BC in 2017 (south of Punta de Mata). The cumulative BC emissions throughout the year for the whole Persian gulf region is shown in Figure 22.

Our best estimate for the global BC emissions from gas flaring is 73.4±36.7 Gg. As for the flared volume, 4 countries account for more than half of that value: Iraq (10.8 Gg), Iran (10.5 Gg), Russia (10.3 Gg) and Algeria (6.0 Gg). This value is about one third of the estimate from the Greenhouse Gas – Air Pollution Interactions and Synergies (GAINS) model (ECLIPSE V5a global emission fields) (Klimont et al., 2017): 270 and 210 Gg in 2005 and 2010, respectively. Such a decrease between 2010 and 2017 may be unlikely, given that the production within the upstram oil and gas (UOG) industry did not decrease in such a significant way. Rather than a decrease in the activity, or a shift in the emission factors (EF), the discrepancy might be due to how the EF is determined (see section 2.3). Assigning the EF at the operational level, for each detection, seems to us

https://doi.org/10.5194/essd-2019-99
Preprint. Discussion started: 25 July 2019

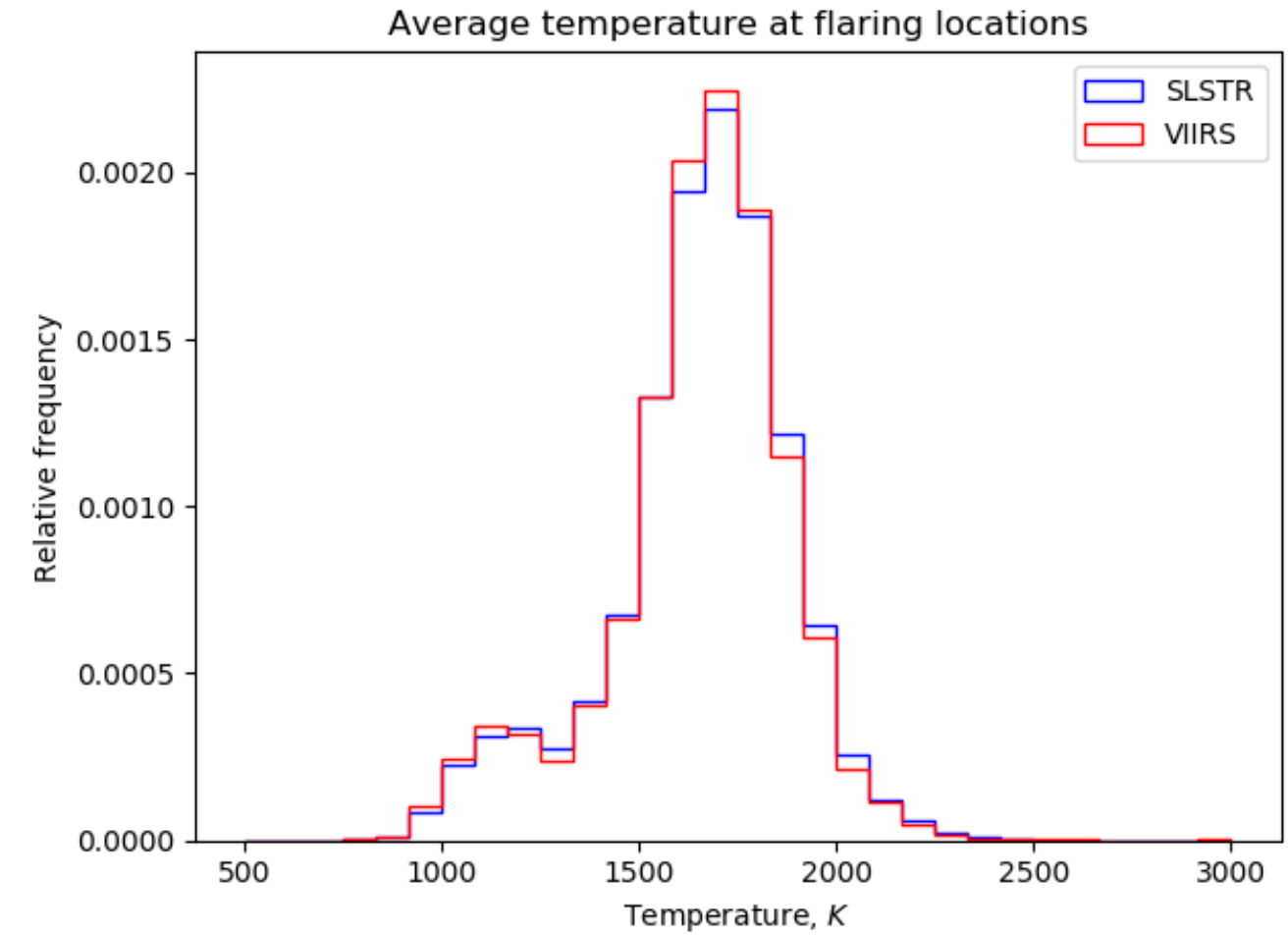

Figure 16. Comparison of the average retrieved temperature at the flaring locations for VIIRS Nightfire (locations shown in Figure 15 in red) and for SLSTR (locations shown in Figure 6 in blue). Relative frequency is used to ensure comparability independently of the total number of observations (6232 flaring locations for SLSTR, 18855 flaring locations for VIIRS Nightfire).

https://doi.org/10.5194/essd-2019-99
Preprint. Discussion started: 25 July 2019

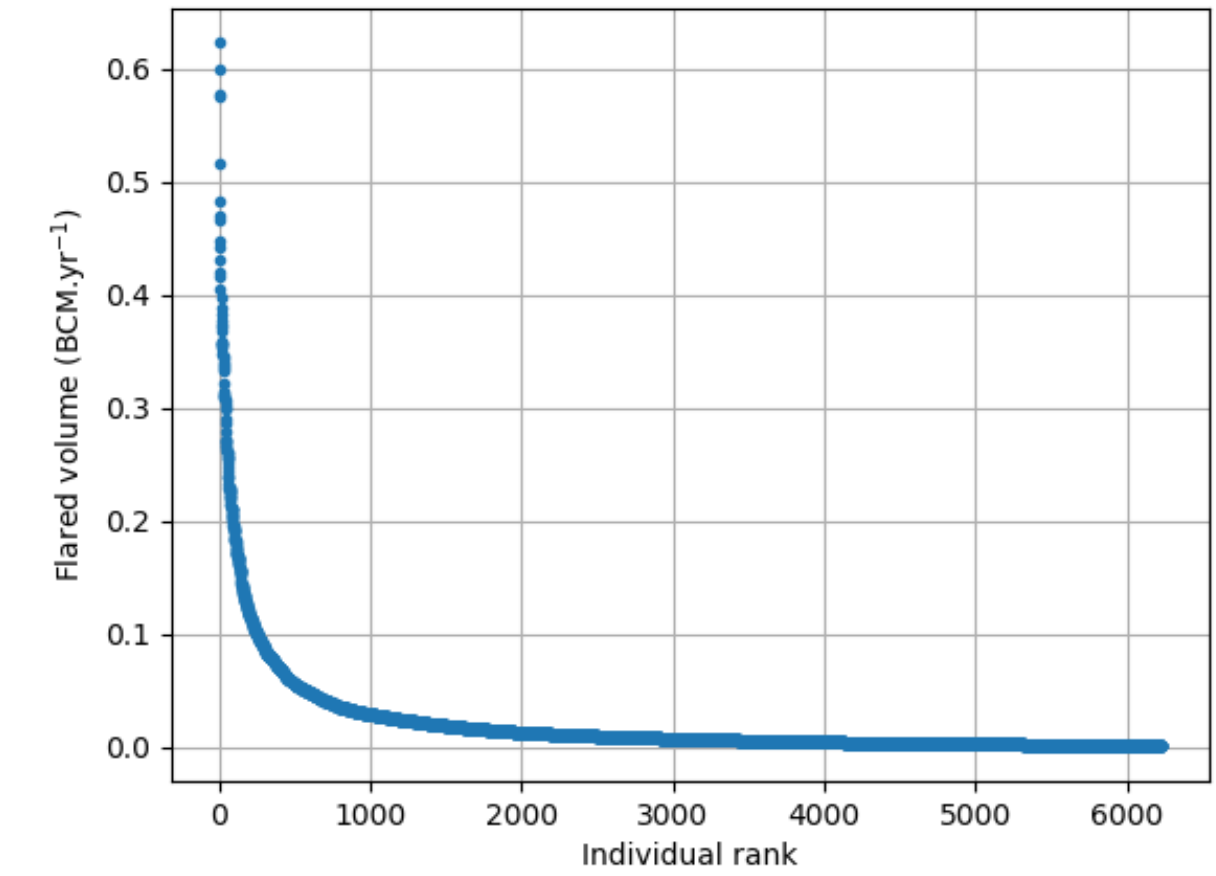

Figure 17. Flaring activity (best estimate, BCM per year) for each individual flaring location (6232 in total).

more realistic than assigning it at the country level. Our global estimate is also larger than the global extrapolation made from a flaring emission study in the Bakken field by Weyant et al. (2016): 20±6 Gg. We believe that our dynamic assignment of the EF, based on the single temperature retrieval, should be closer to reality than globally extrapolating the EF measured at a single field. Huang and Fu (2016) used the VIIRS Nightfire dataset for the flaring activity and emission factors derived from the flared gas chemical composition to compute the BC emissions. Their estimate range from approximately 140 and 200 Gg per year between 1994 and 2012. VIIRS Nightfire was also the basis for the determination of atmospheric emissions from gas flaring by Doumbia et al. (2019) for the African continent. The authors computed a BC emission in 2005 between 6.2 and 141.2 Gg. For the same continent, our results yield 16.1 Gg.

https://doi.org/10.5194/essd-2019-99
Preprint. Discussion started: 25 July 2019

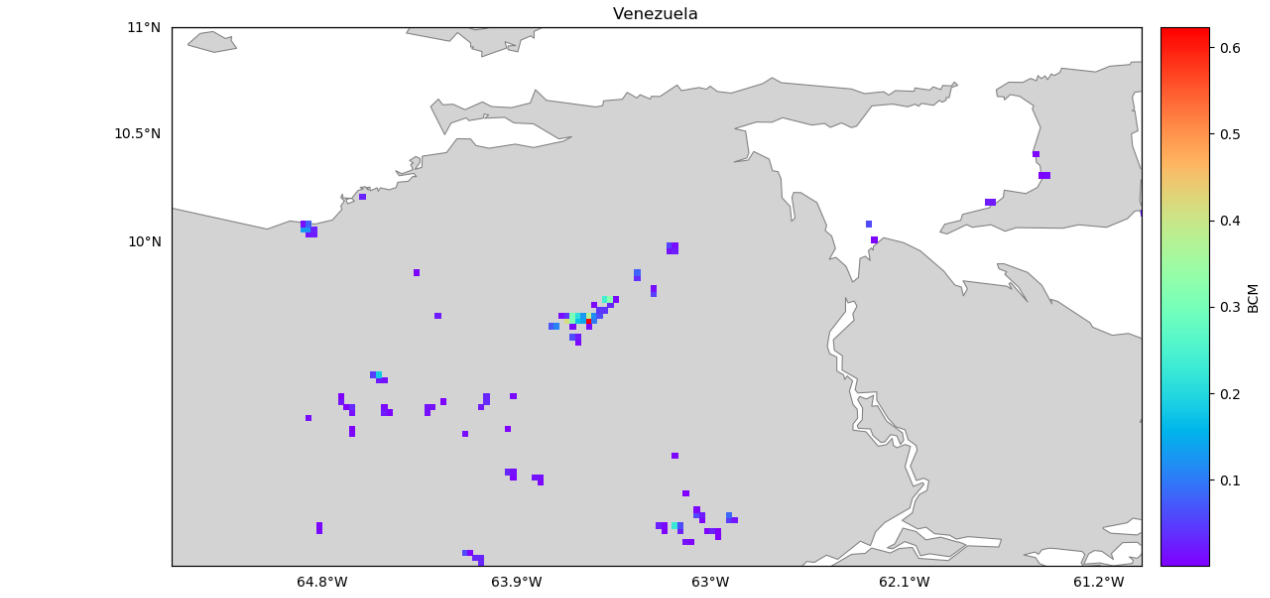

Figure 18. Total flaring activity (best estimate, BCM per year) for each individual flaring location in the oil producing region of Venezuela (112 flaring locations in the region, aggregated from 2391 high accuracy detections over 200 days), where the most active flare is located.

4 Conclusions

In this work we apply a previously described hot spot detection and characterisation procedure (Caseiro et al., 2018) to the 2017 observations of Sentinel-3A's Sea and Land Surface Temperature Radiometer (SLSTR) instrument. We present a new gas flaring discrimination procedure, based on two characteristics of gas flares: persistence and temperature. This allow us to refine the characterisation procedure in order to separate gas flares from other sources of heat emissions. Validation through referencing with high-resolution images yields a detection accuracy of 85±11%, with a commission error of 3±1%.

Our methodology detects 6232 flaring sites worldwide in 2017. Over half of those are located in five countries only: Russia, the United States, Iran, China and Algeria.

Additionally to the detection we present a way to assess the volume of flared gas. This is based on the observed relationship between the flared volume and observed flare radiative energy. The resulting estimate of flared volume allows us to estimate activity from which we can infer emission estimates.

In order to compute the best estimate of activity at the detected flaring sites, we apply a scaling factor, differentiated by latitude, to account for observation gaps (cloud cover and overpass frequency). The upper bound is computed as if the flare would constantly burn for the whole year. The lower bound is computed as if the flare would burn on days with hot spot

https://doi.org/10.5194/essd-2019-99
Preprint. Discussion started: 25 July 2019

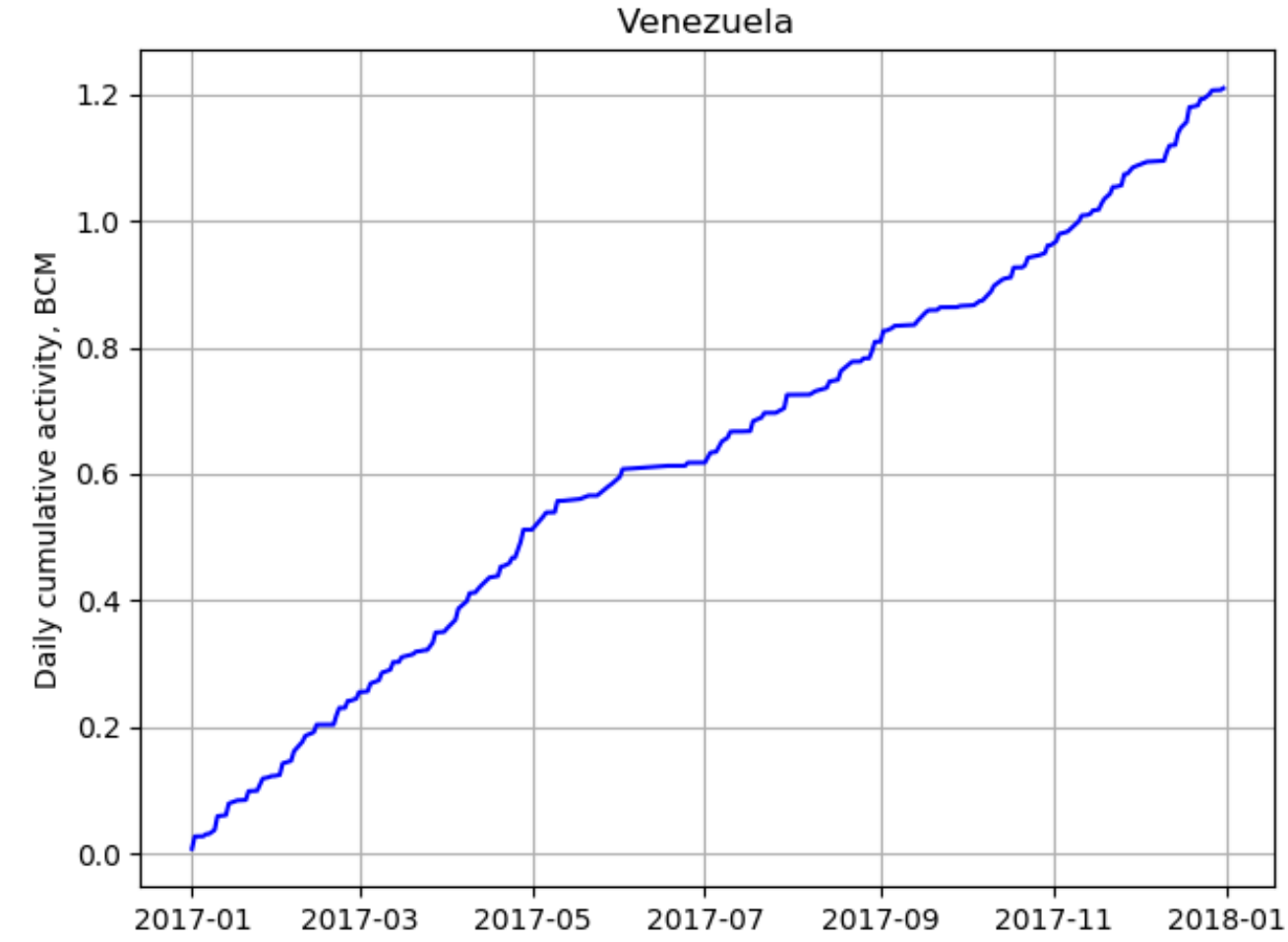

Figure 19. Cumulative total observed flaring activity (BCM_{min}) in the oil and gas producing region of Venezuela (112 flaring locations in the region, aggregated from 2391 high accuracy detections over 200 days), where the most active flare is located.

https://doi.org/10.5194/essd-2019-99
Preprint. Discussion started: 25 July 2019

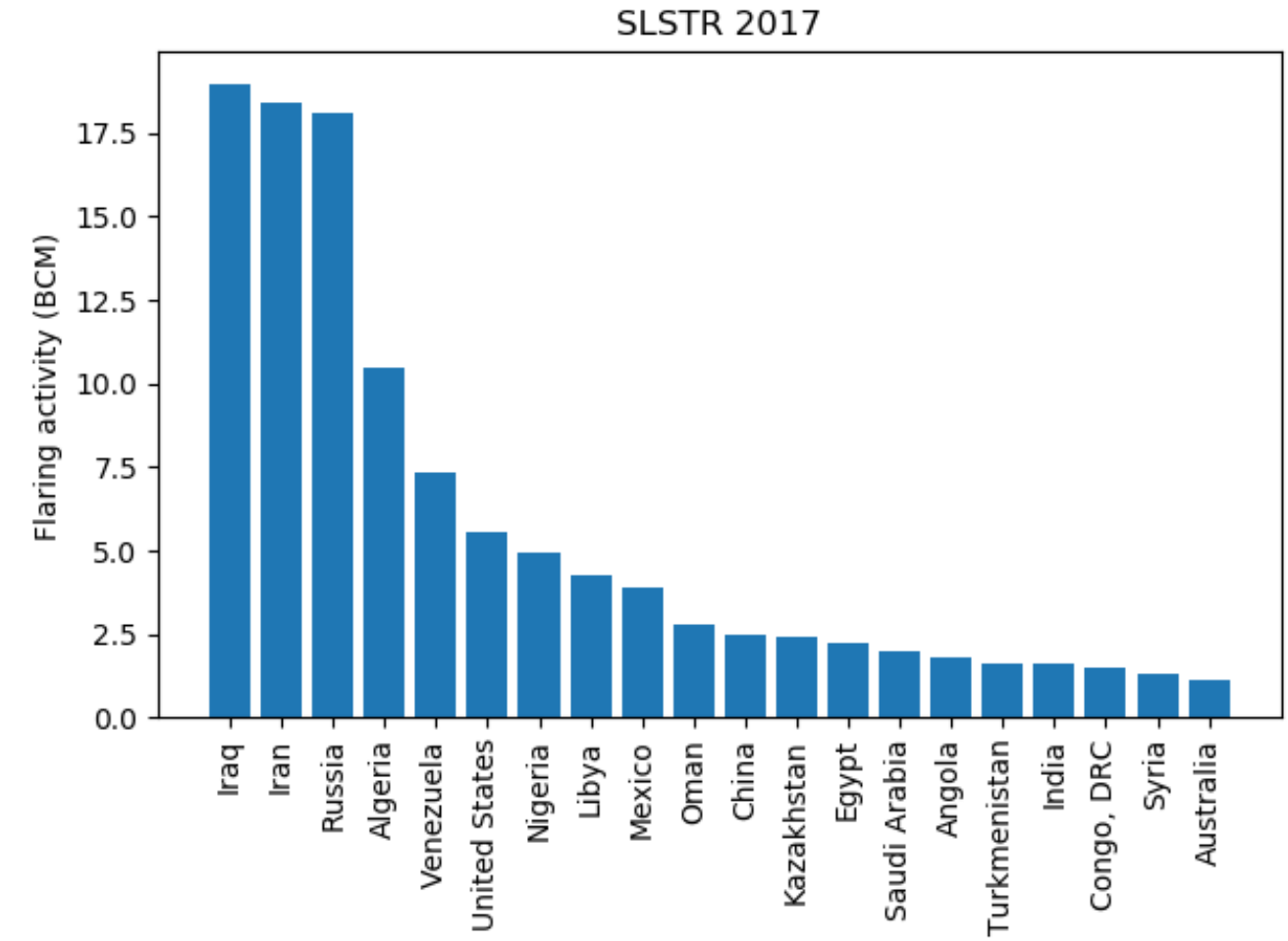

Figure 20. Flaring activity (best estimate, BCM per year) by country, top 20.

detections only. Our analysis yields a result of 129±64 billion cubic metres (BCM) of gas flared in 2017 (best estimate). Only four countries are responsible for half of the global gas flaring activity: Iraq, Iran, Russia and Algeria. The most active flaring location is located in Venezuela and burned 0.623 BCM in 2017.

We further quantify the black carbon (BC) emissions due to gas flaring. We assume that temperature is an indication of the completeness of combustion and use the flame temperature as derived by the hot spot detection and characterisation procedure to determine the emission factor for each single detection, bounded by the range of previously published emission factors. We assume that a temperature close to the adiabatic flame temperature corresponds to the lower bound of the emission factor range considered, while the lowest temperature corresponds to the upper bound. The minimum, maximum and best estimates for the BC emissions are computed in the same way as the flared volume. Our resulting best estimate for the emission of BC to the

https://doi.org/10.5194/essd-2019-99
Preprint. Discussion started: 25 July 2019

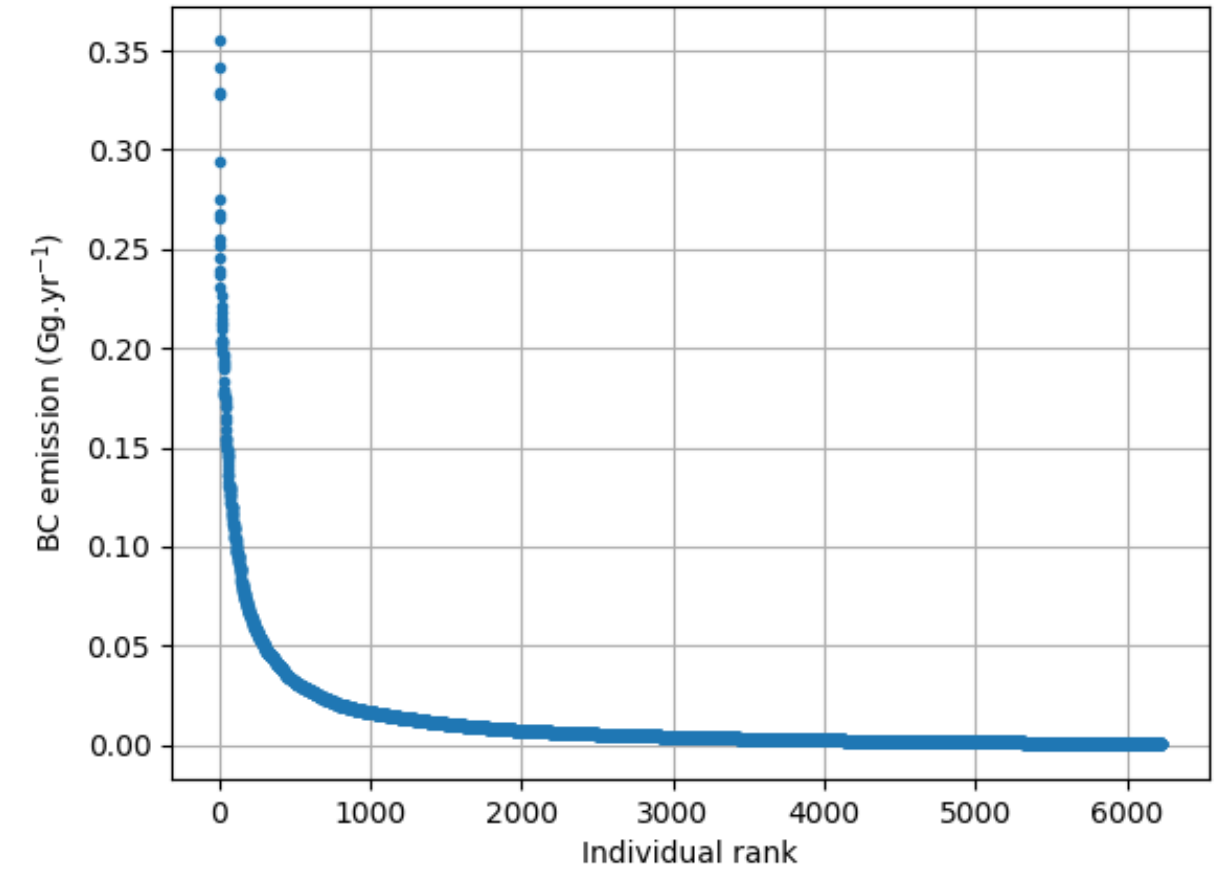

Figure 21. Flaring BC emissions (best estimate, Gg per year) for each individual flaring location (6232 in total).

atmosphere by gas flaring in 2017 is 73.4 Gg. With Iraq, Iran, Russia and Algeria being responsible for roughly one half of those emissions. The most active flaring location, which is also the one with the highest emissions, is estimated to have yearly emission of 0.35 Gg of BC in 2017.

The flaring activity and the related black carbon emissions product are available with 0.025° × 0.025° resolution on the Emissions of atmospheric Compounds and Compilation of Ancillary Data (ECCAD) web site (https://eccad3.sedoo.fr) for use in, e.g., atmospheric composition modelling studies.

https://doi.org/10.5194/essd-2019-99
Preprint. Discussion started: 25 July 2019

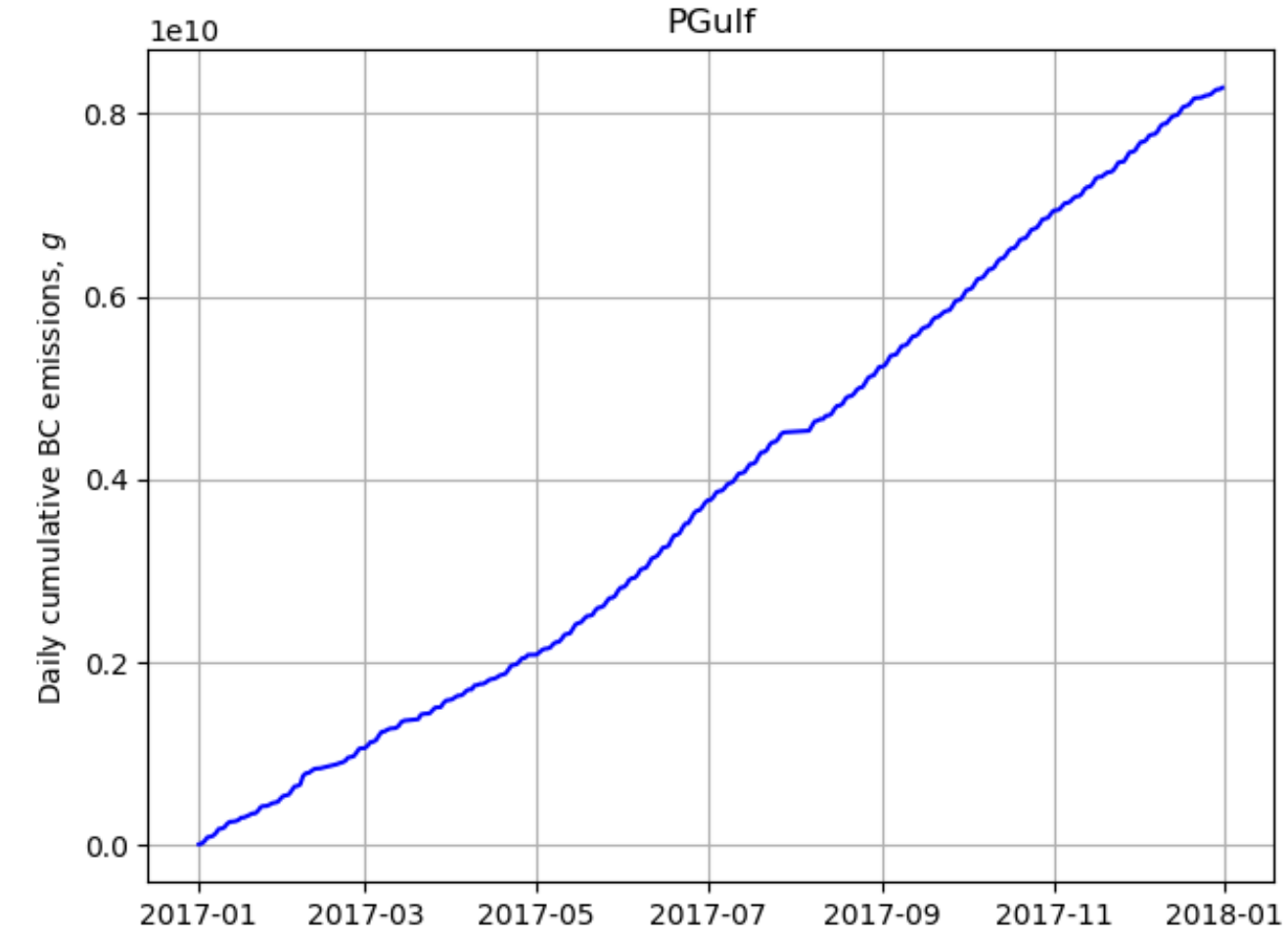

Figure 22. Cumulative total observed BC emissions (BC_{min}, g) in the oil and gas producing region of the Persian gulf, as shown in Figure 10 (1184 flaring locations in the region, aggregated from 41600 high accuracy detections over 348 days).

https://doi.org/10.5194/essd-2019-99
Preprint. Discussion started: 25 July 2019

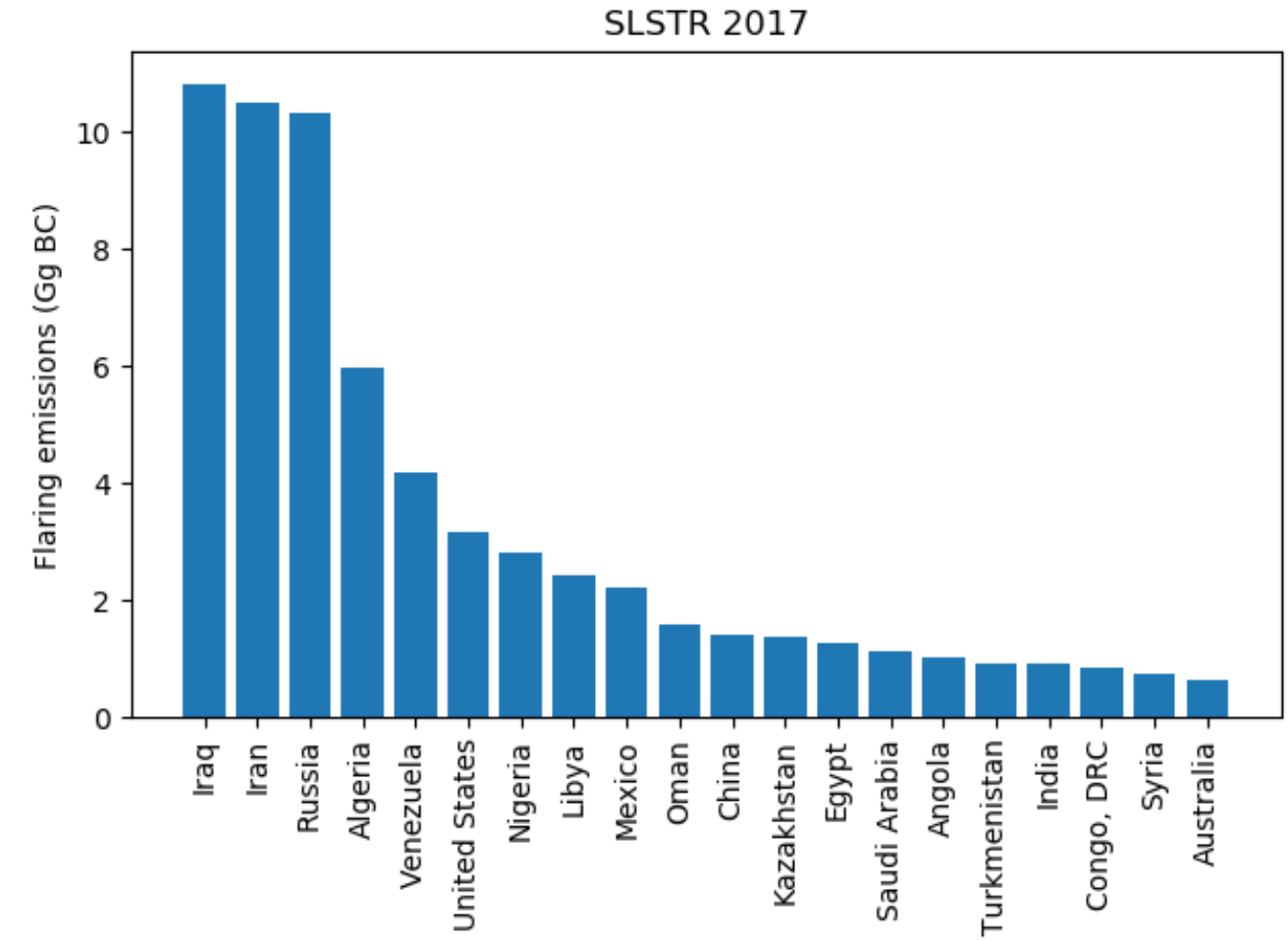

Figure 23. Flaring BC emissions (best estimate, Gg per year) by country, top 20.

5 Data availability

The dataset produced by the described methodology and analysed in this paper is available at https://eccad3.sedoo.fr/#GFlaringS3 with the DOI 10.25326/19 (Caseiro and Kaiser, 2019).

https://doi.org/10.5194/essd-2019-99
Preprint. Discussion started: 25 July 2019

Open Access Earth System Science Data Discussions

Author contributions. Conceptualization, AC and JWK; Methodology, AC and JWK; Software, AC and DL; Validation, AC, JWK and BG; Formal Analysis, Investigation & Resources, AC and BG; Data Curation, AC, BG and JWK; Writing–Original Draft Preparation, AC; Writing—Review & Editing, BG, JWK & GR; Visualization, AC; Supervision, Project Administration & Funding Acquisition, JWK and GR.

Competing interests. The authors declare that there are no competing interests.

Acknowledgements. The data was produced in the project "GFS3 - Identification of gas flares and quantification of their emissions using Sentinel-3 SLSTR" funded by the German Federal Ministry for Economic Affairs and Energy (BMWi, Bundesministerium für Wirtschaft und Energie) under contract number FKZ 50EE1339.

https://doi.org/10.5194/essd-2019-99
Preprint. Discussion started: 25 July 2019

Open Access Earth System Science Data Discussions

References

Ahmed Osama Abdulrahman, Donald Huisingh, and Wim Hafkamp: Sustainability improvements in Egypt's oil & gas industry by implementation of flare gas recovery, Journal of Cleaner Production, 98, 116 – 122, https://doi.org/https://doi.org/10.1016/j.jclepro.2014.11.086, http://www.sciencedirect.com/science/article/pii/S0959652614013894, special Volume: Support your future today! Turn environmental challenges into opportunities., 2015.

Ajao, E. A. and Anurigwo, S.: Land-Based Sources of Pollution in the Niger Delta, Nigeria, Ambio, 13, 442–445, 2002.

Akinola, A. O.: Resource Misgovernance and the Contradictions of Gas Flaring in Nigeria: A Theoretical Conversation, Journal of Asian and African Studies, 53, 749–763, https://doi.org/10.1177/0021909617722374, https://doi.org/10.1177/0021909617722374, 2018.

Anejionu, O. C., Blackburn, G. A., and Whyatt, J. D.: Detecting gas flares and estimating flaring volumes at individual flow stations using {MODIS} data, Remote Sensing of Environment, 158, 81 – 94, https://doi.org/http://dx.doi.org/10.1016/j.rse.2014.11.018, http://www.sciencedirect.com/science/article/pii/S003442571400460X, 2015.

Anejionu, O. C. D., Blackburn, G. A., and Whyatt, J. D.: Satellite survey of gas flares: development and application of a Landsat-based technique in the Niger Delta, International Journal of Remote Sensing, 35, 1900–1925, https://doi.org/10.1080/01431161.2013.879351, http://dx.doi.org/10.1080/01431161.2013.879351, 2014.

Anomohanran, O.: Determination of greenhouse gas emission resulting from gas flaring activities in Nigeria, Energy Policy, 45, 666 – 670, https://doi.org/http://dx.doi.org/10.1016/j.enpol.2012.03.018, http://www.sciencedirect.com/science/article/pii/S0301421512002236, 2012.

Bond, T. C., Doherty, S. J., Fahey, D. W., Forster, P. M., Berntsen, T., DeAngelo, B. J., Flanner, M. G., Ghan, S., K§rcher, B., Koch, D., Kinne, S., Kondo, Y., Quinn, P. K., Sarofim, M. C., Schultz, M. G., Schulz, M., Venkataraman, C., Zhang, H., Zhang, S., Bellouin, N., Guttikunda, S. K., Hopke, P. K., Jacobson, M. Z., Kaiser, J. W., Klimont, Z., Lohmann, U., Schwarz, J. P., Shindell, D., Storelvmo, T., Warren, S. G., and Zender, C. S.: Bounding the role of black carbon in the climate system: A scientific assessment, Journal of Geophysical Research: Atmospheres, 118, 5380–5552, https://doi.org/10.1002/jgrd.50171, http://dx.doi.org/10.1002/jgrd.50171, 2013.

Casadio, S., Arino, O., and Minchella, A.: Use of {ATSR} and {SAR} measurements for the monitoring and characterisation of night-time gas flaring from off-shore platforms: The North Sea test case, Remote Sensing of Environment, 123, 175 – 186, https://doi.org/http://dx.doi.org/10.1016/j.rse.2012.03.021, http://www.sciencedirect.com/science/article/pii/S003442571200140X, 2012a.

Casadio, S., Arino, O., and Serpe, D.: Gas flaring monitoring from space using the {ATSR} instrument series, Remote Sensing of Environment, 116, 239 – 249, https://doi.org/http://dx.doi.org/10.1016/j.rse.2010.11.022, http://www.sciencedirect.com/science/article/pii/S0034425711002240, advanced Along Track Scanning Radiometer(AATSR) Special Issue, 2012b.

Caseiro, A. and Kaiser, J. W.: Global Gas Flaring activity and Black Carbon emissions, data, https://doi.org/10.25326/19, https://permalink.aeris-data.fr/GFlaringS3, 2019.

Caseiro, A., Rücker, G., Tiemann, J., Leimbach, D., Lorenz, E., Frauenberger, O., and Kaiser, J. W.: Persistent Hot Spot Detection and Characterisation Using SLSTR, Remote Sensing, 10, https://doi.org/10.3390/rs10071118, http://www.mdpi.com/2072-4292/10/7/1118, 2018.

Chowdhury, S., Shipman, T., Chao, D., Elvidge, C., Zhizhin, M., and Hsu, F.: Daytime gas flare detection using Landsat-8 multispectral data, in: 2014 IEEE Geoscience and Remote Sensing Symposium, pp. 258–261, https://doi.org/10.1109/IGARSS.2014.6946406, 2014.

https://doi.org/10.5194/essd-2019-99
Preprint. Discussion started: 25 July 2019

Doherty, S. J., Warren, S. G., Grenfell, T. C., Clarke, A. D., and Brandt, R. E.: Light-absorbing impurities in Arctic snow, Atmospheric Chemistry and Physics, 10, 11 647–11 680, https://doi.org/10.5194/acp-10-11647-2010, https://www.atmos-chem-phys.net/10/11647/2010/, 2010.

Doumbia, E. H. T., Liousse, C., Keita, S., Granier, L., Granier, C., Elvidge, C. D., Elguindi, N., and Law, K.: Flaring emissions in Africa: Distribution, evolution and comparison with current inventories, Atmospheric Environment, 199, 423 – 434, https://doi.org/https://doi.org/10.1016/j.atmosenv.2018.11.006, http://www.sciencedirect.com/science/article/pii/S1352231018307726, 2019.

Elvidge, C. D., Imhoff, M. L., Baugh, K. E., Hobson, V. R., Nelson, I., Safran, J., Dietz, J. B., and Tuttle, B. T.: Night-time lights of the world: 1994,Äì1995, {ISPRS} Journal of Photogrammetry and Remote Sensing, 56, 81 – 99, https://doi.org/http://dx.doi.org/10.1016/S0924-2716(01)00040-5, http://www.sciencedirect.com/science/article/pii/S0924271601000405, 2001.

Elvidge, C. D., Baugh, K. E., Tuttle, B. T., Howard, A. T., Pack, D. W., Milesi, C., and Erwin, E. H.: A Twelve Year Record of National and Global Gas Flaring Volumes Estimated Using Satellite Data, Tech. rep., World Bank, 2007.

Elvidge, C. D., Baugh, K., Tuttle, B., Ziskin, D., Ghosh, T., Zhizhin, M., and Pack, D.: Improving Satellite Data Estimation of Gas Flaring Volumes, Tech. rep., GGFR - World Bank, 2009.

Elvidge, C. D., Zhizhin, M., Hsu, F.-C., and Baugh, K. E.: VIIRS Nightfire: Satellite Pyrometry at Night, Remote Sensing, 5, 4423–4449, https://doi.org/10.3390/rs5094423, http://www.mdpi.com/2072-4292/5/9/4423, 2013.

Elvidge, C. D., Zhizhin, M., Baugh, K., Hsu, F.-C., and Ghosh, T.: Methods for Global Survey of Natural Gas Flaring from Visible Infrared Imaging Radiometer Suite Data, Energies, 9, 14, https://doi.org/10.3390/en9010014, http://www.mdpi.com/1996-1073/9/1/14, 2016.

Elvidge, C. D., Bazilian, M. D., Zhizhin, M., Ghosh, T., Baugh, K., and Hsu, F.-C.: The potential role of natural gas flaring in meeting greenhouse gas mitigation targets, Energy Strategy Reviews, 20, 156 – 162, https://doi.org/https://doi.org/10.1016/j.esr.2017.12.012, http://www.sciencedirect.com/science/article/pii/S2211467X17300962, 2018.

Emeka Ojijiagwo, Chike F. Oduoza, and Nwabueze Emekwuru: Economics of gas to wire technology applied in gas flare management, Engineering Science and Technology, an International Journal, 19, 2109 – 2118, https://doi.org/https://doi.org/10.1016/j.jestch.2016.09.012, http://www.sciencedirect.com/science/article/pii/S2215098616307765, 2016.

Evangeliou, N., Shevchenko, V. P., Yttri, K. E., Eckhardt, S., Sollum, E., Pokrovsky, O. S., Kobelev, V. O., Korobov, V. B., Lobanov, A. A., Starodymova, D. P., Vorobiev, S. N., Thompson, R. L., and Stohl, A.: Origin of elemental carbon in snow from western Siberia and northwestern European Russia during winter–spring 2014, 2015 and 2016, Atmospheric Chemistry and Physics, 18, 963–977, https://doi.org/10.5194/acp-18-963-2018, https://www.atmos-chem-phys.net/18/963/2018/, 2018.

Faruolo, M., Coviello, I., Filizzola, C., Lacava, T., Pergola, N., and Tramutoli, V.: A satellite-based analysis of the Val d'Agri Oil Center (southern Italy) gas flaring emissions, Natural Hazards and Earth System Science, 14, 2783–2793, https://doi.org/10.5194/nhess-14-2783-2014, http://www.nat-hazards-earth-syst-sci.net/14/2783/2014/, 2014.

Faruolo, M., Lacava, T., Pergola, N., and Tramutoli, V.: On the Potential of the RST-FLARE Algorithm for Gas Flaring Characterization from Space, Sensors, 18, https://doi.org/10.3390/s18082466, http://www.mdpi.com/1424-8220/18/8/2466, 2018.

Flanner, M. G., Zender, C. S., Randerson, J. T., and Rasch, P. J.: Present-day climate forcing and response from black carbon in snow, Journal of Geophysical Research: Atmospheres, 112, https://doi.org/10.1029/2006JD008003, https://agupubs.onlinelibrary.wiley.com/doi/abs/10.1029/2006JD008003, 2007.

https://doi.org/10.5194/essd-2019-99
Preprint. Discussion started: 25 July 2019

Franklin, M., Chau, K., Cushing, L. J., and Johnston, J. E.: Characterizing Flaring from Unconventional Oil and Gas Operations in South Texas Using Satellite Observations, Environmental Science & Technology, 0, null, https://doi.org/10.1021/acs.est.8b05355, https://doi.org/10.1021/acs.est.8b05355, pMID: 30657671, 2019.

Gabriele Comodi, Massimiliano Renzi, and Mosè Rossi: Energy efficiency improvement in oil refineries through flare gas recovery technique to meet the emission trading targets, Energy, 109, 1 – 12, https://doi.org/https://doi.org/10.1016/j.energy.2016.04.080, http://www.sciencedirect.com/science/article/pii/S0360544216304935, 2016.

Hansen, J. and Nazarenko, L.: Soot climate forcing via snow and ice albedos, Proceedings of the National Academy of Sciences, 101, 423–428, https://doi.org/10.1073/pnas.2237157100, http://www.pnas.org/cgi/doi/10.1073/pnas.2237157100, 2004.

Heinrich, U., Dungworth, D. L., Pott, F., Peters, L., Dasenbrock, C., Levsen, K., Koch, W., Creutzenberg, O., and Schulte, A.: The Carcinogenic Effects of Carbon Black Particles and Tar,ÄìPitch Condensation Aerosol after Inhalation Exposure of Rats, Annals of Occupational Hygiene, 38, 351–356, https://doi.org/10.1093/annhyg/38.inhaled_particles_VII.351, http://annhyg.oxfordjournals.org/content/38/inhaled_particles_VII/351.abstract, 1994.

Huang, K. and Fu, J. S.: A global gas flaring black carbon emission rate dataset from 1994 to 2012, Scientific Data, 3, https://doi.org/10.1038/sdata.2016.104, http://dx.doi.org/10.1038/sdata.2016.104, 2016.

Huang, K., Fu, J. S., Prikhodko, V. Y., Storey, J. M., Romanov, A., Hodson, E. L., Cresko, J., Morozova, I., Ignatieva, Y., and Cabaniss, J.: Russian anthropogenic black carbon: Emission reconstruction and Arctic black carbon simulation, Journal of Geophysical Research: Atmospheres, 120, 11,306–11,333, https://doi.org/10.1002/2015JD023358, http://dx.doi.org/10.1002/2015JD023358, 2015JD023358, 2015.

IPCC: Climate Change 2013: The Physical Science Basis. Contribution of Working Group I to the Fifth Assessment Report of the Intergovernmental Panel on Climate Change, Cambridge University Press, Cambridge, United Kingdom and New York, NY, USA, https://doi.org/10.1017/CBO9781107415324, www.climatechange2013.org, 2013.

Ismail, O. and Umukoro, G.: Global Impact of Gas Flaring, Energy and Power Engineering, 4, 290 – 302, https://doi.org/10.4236/epe.2012.44039, http://www.scirp.org/journal/PaperInformation.aspx?PaperID=20231#.VZvUq8789Ro, 2012.

Julius, O. O.: Environmental impact of gas flaring within Umutu-Ebedei gas plant in Delta State, Nigeria, Archives of Applied Science Research, 3, 272–279, 2011.

Klimont, Z., Kupiainen, K., Heyes, C., Purohit, P., Cofala, J., Rafaj, P., Borken Kleefeld, J., and Schöpp, W.: Global anthropogenic emissions of particulate matter including black carbon, Atmospheric Chemistry and Physics, 17, 8681–8723, https://doi.org/10.5194/acp-17-8681-2017, https://www.atmos-chem-phys.net/17/8681/2017/, 2017.

Li, C., Hsu, N. C., Sayer, A. M., Krotkov, N. A., Fu, J. S., Lamsal, L. N., Lee, J., and Tsay, S.-C.: Satellite observation of pollutant emissions from gas flaring activities near the Arctic, Atmospheric Environment, 133, 1 – 11, https://doi.org/http://dx.doi.org/10.1016/j.atmosenv.2016.03.019, http://www.sciencedirect.com/science/article/pii/S1352231016301893, 2016.

Liu, Y., Hu, C., Zhan, W., Sun, C., Murch, B., and Ma, L.: Identifying industrial heat sources using time-series of the VIIRS Nightfire product with an object-oriented approach, Remote Sensing of Environment, 204, 347 – 365, https://doi.org/https://doi.org/10.1016/j.rse.2017.10.019, http://www.sciencedirect.com/science/article/pii/S0034425717304820, 2018.

McEwen, J. D. and Johnson, M. R.: Black carbon particulate matter emission factors for buoyancy-driven associated gas flares, Journal of the Air & Waste Management Association, 62, 307–321, https://doi.org/10.1080/10473289.2011.650040, http://dx.doi.org/10.1080/10473289.2011.650040, 2012.

https://doi.org/10.5194/essd-2019-99
Preprint. Discussion started: 25 July 2019

Nwaichi, E. and Uzazobona, M.: Estimation of the CO_2 Level due to Gas Flaring in the Niger Delta, Research Journal of Environmental Sciences, 5, 565–572, https://doi.org/10.3923/rjes.2011.565.572, http://scialert.net/abstract/?doi=rjes.2011.565.572, 2011.

Nwoye, C. I., Nwakpa, S. O., Nwosu, I. E., Odo, J. U., Chinwuko, E. C., and Idenyi, N. E.: Multi-Factorial Analysis of Atmospheric Noise Pollution Level Based on Emitted Carbon and Heat Radiation during Gas Flaring, Journal of Atmospheric Pollution, 2, 22–29, https://doi.org/10.12691/jap-2-1-5, http://pubs.sciepub.com/jap/2/1/5, 2014.

Obioh, I., Oluwole, A. F., and Akeredolu, F. A.: Non-CO_2 gaseous emissions from upstream oil and gas operations in Nigeria, Environmental Monitoring and Assessment, 31, 67–72, 1994.

Olivier, J., Janssens Maenhout, G., Muntean, M., and Peters, J.: Trends in global CO2 emissions: 2014 Report, Tech. rep., European Commission, Joint Research Centre (JRC), Institute for Environment and Sustainability (IES), PBL Netherlands Environmental Assessment Agency, The Hague, 2014.

Onu, P. u., Quan, X., and Ling, X.: Acid rain: an analysis on the cause, impacts and abatement measures Niger Delta perspective, Nigeria., International Journal of Scientific & Engineering Research, 5, 1214–1219, 2014.

Papailias, G. and Mavroidis, I.: Atmospheric Emissions from Oil and Gas Extraction and Production in Greece, Atmosphere, 9, https://doi.org/10.3390/atmos9040152, http://www.mdpi.com/2073-4433/9/4/152, 2018.

Quinn, P. K., Shaw, G., Andrews, E., Dutton, E. G., Ruoho Airola, T., and Gong, S. L.: Arctic haze: current trends and knowledge gaps, Tellus B, 59, 99–114, https://doi.org/10.1111/j.1600-0889.2006.00238.x, http://dx.doi.org/10.1111/j.1600-0889.2006.00238.x, 2007.

Rahimpour, M. R. and Jokar, S. M.: Feasibility of flare gas reformation to practical energy in Farashband gas refinery: No gas flaring, Journal of Hazardous Materials, 209,Äì210, 204 – 217, https://doi.org/http://dx.doi.org/10.1016/j.jhazmat.2012.01.017, http://www.sciencedirect.com/science/article/pii/S0304389412000337, 2012.

Schwarz, J. P., Holloway, J. S., Katich, J. M., McKeen, S., Kort, E. A., Smith, M. L., Ryerson, T. B., Sweeney, C., and Peischl, J.: Black Carbon Emissions from the Bakken Oil and Gas Development Region, Environmental Science & Technology Letters, 2, 281–285, https://doi.org/10.1021/acs.estlett.5b00225, https://doi.org/10.1021/acs.estlett.5b00225, 2015.

Serreze, M. C. and Barry, R. G.: Processes and impacts of Arctic amplification: A research synthesis, Global and Planetary Change, 77, 85 – 96, https://doi.org/https://doi.org/10.1016/j.gloplacha.2011.03.004, http://www.sciencedirect.com/science/article/pii/S0921818111000397, 2011.

Siebert, L., Simkin, T., and Kimberly, P.: Volcanoes of the World: Third Edition, University of California Press, 3 edn., http://www.jstor.org/stable/10.1525/j.ctt1pnqdx, 2010.

Stohl, A., Klimont, Z., Eckhardt, S., Kupiainen, K., Shevchenko, V. P., Kopeikin, V. M., and Novigatsky, A. N.: Black carbon in the Arctic: the underestimated role of gas flaring and residential combustion emissions, Atmospheric Chemistry and Physics, 13, 8833–8855, https://doi.org/10.5194/acp-13-8833-2013, http://www.atmos-chem-phys.net/13/8833/2013/, 2013.

Uzomah, V. and Sangodoyin, A.: Rainwater chemistry as influenced by atmospheric deposition of pollutants in Southern Nigeria, Environmental Management and Health, 11, 149–156, https://doi.org/10.1108/09566160010321569, https://doi.org/10.1108/09566160010321569, 2000.

Venzke, E.: Global Volcanism Program – Volcanoes of the World, v. 4.7.4. Smithsonian Institution. Downloaded 02 Oct 2018, https://doi.org/10.5479/si.GVP.VOTW4-2013, 2013.

Weyant, C. L., Shepson, P. B., Subramanian, R., Cambaliza, M. O. L., Heimburger, A., McCabe, D., Baum, E., Stirm, B. H., and Bond, T. C.: Black Carbon Emissions from Associated Natural Gas Flaring, Environmental Science & Technology, 50, 2075–2081, https://doi.org/10.1021/acs.est.5b04712, http://dx.doi.org/10.1021/acs.est.5b04712, pMID: 26764563, 2016.

https://doi.org/10.5194/essd-2019-99
Preprint. Discussion started: 25 July 2019

Open Access Earth System Science Data Discussions

Zolfaghari, M., Pirouzfar, V., and Sakhaeinia, H.: Technical characterization and economic evaluation of recovery of flare gas in various gas-processing plants, Energy, 124, 481 – 491, https://doi.org/https://doi.org/10.1016/j.energy.2017.02.084, http://www.sciencedirect.com/science/article/pii/S036054421730258X, 2017.